Multiobjective Optimisation of Hybrid Wind-PV-Battery-Fuel Cell-Electrolyser-Diesel Systems: An Integrated Configuration-Size Formulation Approach

Alireza Maheri[1,2,*], Ibrahim Unsal[3], Omid Mahian[4,**]
[1]School of Engineering, University of Aberdeen, Aberdeen, UK
[2]Centre for Energy Transition, University of Aberdeen, Aberdeen, UK
[3]Faculty of Engineering, Northumbria University, Newcastle upon Tyne, UK
[4] School of Chemical Engineering and Technology, Xi'an Jiaotong University, Xi'an, China
* Corresponding author E-Mail: alireza.maheri@abdn.ac.uk
** Corresponding author E-Mail: omid.mahian@gmail.com

Abstract
A generic integrated configuration-size optimisation formulation for design of hybrid renewable energy systems (HRES) is presented in this paper. This formulation allows identifying the optimum configuration for a given site and the optimum size of each component in that configuration by solving only one optimisation problem. Single and multiobjective case studies are defined for both on-grid and standalone systems using wind turbine, PV panel, battery bank, fuel cell, electrolyser and diesel generator as potential components. To solve the optimisation problems a genetic algorithm (GA) and a nondominated sorting GA (NSGA-II) are developed, in which the reproduction operators are designed carefully for robust exploration and exploitation at both size and configuration levels. Eight single and multiobjective case studies for a variety of renewable resources, objectives and constraints are conducted. The results show the versatility of the problem formulation in defining different HRES design problems and the robustness of the developed GA and NSGA-II in search within the design space at both configuration and size levels and finding the optimum size and configuration simultaneously.

Keywords: integrated design; hybrid renewable energy systems; GA; NSGA-II; optimisation; MOHRES

1 Introduction
Size optimisation of hybrid renewable energy systems (HRES) is one of the branches of research on HRES, which has received significant attention from the research community. A review of the recently published literature in this field shows that researchers have taken different approaches and methods in (i) problem formulation, (ii) HRES analysis, and (iii) optimisation method.

Problem formulation depends on the type and the number of design variables, objectives and constraints included in the optimisation problem. In the context of size optimisation of HRES, design variables are the size of components in the configuration. Almost all technologically feasible configurations have been the subject of recent studies for power and combined heat and power generation. While the majority of the publications have reported a single objective optimisation, there is an increasing trend for adopting multiobjective optimisation approach in more recent publications. Optimisation method adapted for size optimisation of HRES has been under the influence of the analysis method and the problem formulation. Genetic Algorithm (GA) and Particle Swarm (PS), and their multiobjective variations seem to be the most popular metaheuristic methods for this field.

Analysis of HRES varies from one study to another, depending on the methodological approach in system characterisation, the level of details of cost and power models, and the performance measures of interest. In terms of handling the uncertainties in the demand load, renewable resources, and models, the reported studies have taken two approaches, namely, deterministic or nondeterministic. While the majority of the published works are based on deterministic approaches, some researchers have adopted a nondeterministic approach more recently.

Atieh et al [1] included PV, battery bank, and diesel generator in their study. They used a GA to find the optimum size of these components by considering the total lifespan cost (TLSC) as the objective. Ismail et al [2] also used GA to solve their PV-Battery-Diesel size optimisation problem, but with levelised cost of energy (LCE) as the optimisation objective. Samy et al [3] conducted size optimisation for PV-Fuel cell configuration using PS, Flower Pollination, and Artificial Bee Colony as their single-objective optimisation methods. They used total annual cost (TAC) and loss of power supply probability (LPSP) as objectives. Senthil Kumar et al [4] also reported a size optimisation of PV-Fuel cell configuration by using Nelder-Mead algorithm and a hybrid method as their optimisation algorithm. Mahmoudimehr and Shabani conducted a multiobjective size optimisation for a PV- Pumped hydro configuration [5]. They considered net present value (NPV) and LPSP as the optimisation objectives and used a Nondominated Sorting Genetic Algorithm (NSGA) as the search method. Mohamed et al [6] used a GA with TAC as the objective to solve the size optimisation of a PV-Wind configuration. PV-Wind-Battery is one of the most studied configurations [7-16]. Acuna et al [7] conducted a multiobjective size optimisation, with NPV, LPSP, and LCE as objectives. They used NSGA as their optimisation method. Ahmadi and Abdi conducted a single objective size optimisation of PV-Wind-Battery system with LCE as the objective using big-bang big- crunch method [8]. Fetanatand Khorasaninejad [9] used an Ant Colony algorithm for size optimization of PV-Wind-Battery configuration in a continuous domain with the objective of LCE. They used a continuous domain. Another example of multiobjective size optimisation of PV-Wind-Battery systems with NPV, LPSP, and LCE as objectives, is reported in Ghorbani et al [10]. They used multiobjective PS to solve the problem. [11] conducted single objective size optimisation using the tool DER-CAM for LCE and CO2 emission. Kamjoo et al [12] used deficiency of power supply probability (DPSP) and system cost as two objectives of their multiobjective size optimisation. The works reported in [13, 14, 15, and 16] are other examples of single objective size optimisation of PV-Wind-Battery configuration, in which LCE is used as the optimisation objective. The optimisation methods, however, are different: Bee Swarm algorithm [13], built-in optimiser in HOMER [14], PS and Harmony Search algorithms [15], and a hybrid GA-exhaustive search method [16]. PV-Wind-Battery-Diesel is another well-studied configuration, mainly as a standalone HRES [17-25]. In [17], a hybrid Harmony Search-Simulated Annealing optimisation algorithm is used to minimise the LCE of the system with bio-diesel. TLSC is the optimisation objective for PV-Wind-Battery-Diesel size optimisations reported in [18, 19, and 20] using different optimisation methods: response surface [18], PS [19], and GA [20]. Ogunjuyigbe et al [21] used a single objective GA to find the optimal size of a PV-Wind-Battery-Diesel system which satisfies a set of constraints on TLSC, CO2 emission, and the excess power. LCE and renewable penetration are the objectives of the PV-Wind-Battery-Diesel multiobjective size optimisations reported in [22]. References [23, 24, and 25] also report the results of multiobjective size optimisation of PV-Wind-Battery-Diesel configuration with LCE and LPSP [23]; LCE, NPV, and LPSP [24]; and LCE, LPSP, and renewable penetration [25] as objectives. Maheri [26], Sharafi and

ELMekkawy [27], and Maleki and Pourfayaz [28] considered PV-Wind-Battery-Diesel-Fuel cell configuration in their studies. In [26] using a GA with the objectives of TLSC and unmet load, the effect of dispatch strategy on the performance of hybrid wind-PV-battery-diesel-fuel cell systems was studied. In [27], a combination of TLSC, unmet load, and emission serves as an aggregate objective function for the PS algorithm to find the optimum size of each component in the HRES. Maleki and Pourfayaz used LCE as the objective and used a harmony search algorithm in their study reported in [28]. Other system configurations which have been studied include PV-Wind-Battery- Fuel cell [29], PV-Wind-Biomass [30], PV-Wind-Biomass-Biodiesel [31], PV-Wind-Battery-Thermal storage [32], PV-Wind-Diesel [33], PV-Wind-Fuel cell [34], PV-Wind-Pumped hydro [35], PV-Wind-Solar heat collector-Biomass-Heat pump-Thermal storage [36], Wind-Battery-Diesel [37], Wind-Fuel cell [38], PV-Wind-Electric vehicle [39], Wind-PV- Thermal storage tank [40], and PV-Hydrogen storage-Fuel cell -Solar Thermal [41]. Besides power and combined heat and power generation, size optimisation of renewable and storage systems can be defined in the context of energy transition and system integration scenarios, for instance, renewable-based heating sector [42], cross-sectoral integration of HRES [43], smart energy integration [44], and energy planning [45]. Besides the cost and reliability-rated objectives, CO2 emission and renewable penetration are commonly used objectives in size optimisation of hybrid renewable-nonrenewable systems [46-49].

In all reported research dealing with the optimisation of HRES, the configuration of the system is decided prior to the size optimisation. In other words, design of a HRES takes place in two sequential stages. First the configuration of the system and the type of renewable, non-renewable and storage/auxiliary components are decided. In the second stage, the optimum size of each component in the system is found. A sequential design optimisation has a major drawback. In many cases the decision on the configuration cannot be made unless a detailed cost-benefit analysis is carried out. In such cases, for each possible configuration a size optimisation problem must be solved to determine the optimal cost-related and reliability-related performance measures for that configuration. Once the optimal design of all possible configurations is done, the best configuration can be identified. This, however, can be a cumbersome task. For instance, there are 21 possible configurations with at least one renewable and one auxiliary/storage component which can be made with wind turbine, PV panel, battery bank, fuel cell/electrolyser and diesel generator as potential components.

On the other hand, an integrated configuration-size optimisation formulation has a clear advantage to the current practice, in which the size optimisation is conducted for a pre-defined and not-necessarily optimum configuration or all potential configurations. This paper presents an integrated configuration-size optimisation formulation, which allows finding the optimum configuration for a given site and application, and the optimum size of each component in that configuration by solving only one optimisation problem.

All the optimisation methods reported in the literature are designed and tested for size optimisation problems only and therefore are not robust enough for solving an integrated configuration-size optimisation problem. In an integrated configuration-size optimisation problem the search in the design space must take place at both configuration and size levels. Novel genetic reproduction operators which are designed specifically for simultaneous exploration and exploitation at both levels are also developed and presented in this paper.

2 Integrated Configuration-Size Formulation

Following common practice in formulating an optimisation problem, this section starts by defining the design variables in Section 2.1 and then in Section 2.2 elaborates on the design space, or in other words, the realistic bounds for design variables in which we search for optimum solution(s). The basis of the proposed integrated configuration-size optimisation formulation is explained in this section. In Section 2.3 the design qualities of the problem at hand, here, the performance measure of hybrid renewable energy systems, are defined. The system model, correlating the design variables to the design qualities are also given in this section after defining each performance measure. Finally, in Section 2.4 the optimisation problem is formulated in standard format and is reported.

2.1 Design Variables

In integrated configuration-size optimisation, starting from a generic configuration (in this study wind-PV-fuel cell-electrolyser-diesel-battery bank configuration), the vector of design variables is defined as:

$$\vec{X} = \{n_{WT}, R_{WT}, A_{PV}, n_B, P_{D,nom}, P_{FC,nom}, P_{EL,nom}\} \quad (1)$$

where, n_{WT} stands for the number of wind turbines, R_{WT} is the wind turbine rotor radius (representing the size of the wind turbine), A_{PV} is the total size of the PV panels, n_B stands for the number of batteries, and $P_{D,nom}$, $P_{FC,nom}$ and $P_{EL,nom}$, respectively, are the nominal power of the diesel generator, fuel cell and electrolyser.

It should be noted that, as explained below, there are cases that one of the design variables associated to wind energy (n_{WT}, R_{WT}) is excluded from the vector of design variables. If the wind turbine to be used in the system is known, then R_{WT} is known and fixed, leaving $n_{WT} \geq 0$ as the only design variable to be decided. If the wind turbine has not been decided prior to the optimisation, and if the optimum amount of wind energy can be delivered by one wind turbine, then $n_{WT} = 1$ and fixed, leaving R_{WT} as the remaining design variable to be found. It is a well-known fact that the levelised cost of wind energy reduces with the size of wind turbine. That is, one wind turbine with a nominal power of P is cheaper than n wind turbines, each with a nominal power of P/n. If the wind turbine has not been decided prior to the optimisation, and if the optimum amount of wind energy cannot be delivered by one wind turbine, then both n_{WT} and R_{WT} are design variables.

2.2 Search Space

These design variables are assumed to be bounded between the following ultimate lower and upper limits:

$$\vec{X}^l = \{n_{WT}^l, 0,0,0,0,0,0\} \quad (2.a)$$

where, as explained above:

$$n_{WT}^l = \begin{cases} 0 & if \ \ wind\ turbine\ is\ known \\ 1 & if \ \ wind\ turbine\ is\ not\ known \end{cases} \quad (2.b)$$

$$\vec{X}^u = \{n_{WT}^u, R_{WT}^u, A_{PV}^u, n_B^u, P_{D,nom}^u, P_{FC,nom}^u, P_{EL,nom}^u\} \quad (3)$$

Using the ultimate upper and lower limits as given by Equations 2 and 3, the optimisation process explores a generic configuration including all components. However, within the optimisation process, the size of components which cannot produce/store energy efficiently approach zero, leading to their exclusion from the configuration. In other words, the configuration is obtained via a full cost/performance analysis and an integrated configuration-size optimisation rather than just being selected by the designer.

The upper limits for design variables $\vec{X}^u$ must be selected carefully. On one hand, we want to ensure that the search space is large enough to include all potential optimum solutions, while on the other hand we want to increase the robustness of the search process by avoiding search in unrealistic/infeasible part of the search domain.

In this study, the upper limit for the wind turbine rotor radius R_{WT}^u and the upper limit for the number of wind turbines n_{WT}^u are calculated based on the assumption that the wind turbine(s), by its own, can produce enough power to supply the demand load. This assumption leads to:

$$R_{WT}^u = \sqrt{\frac{L_{max}}{0.5\rho\pi V_{min}^3 C_p \eta_{EM}}} \quad (4.a)$$

and

$$n_{WT}^u = \left[\!\left[\frac{L_{max}}{0.5\rho\pi \left(R_{WT}^u\right)^2 V_{min}^3 C_p \eta_{EM}}\right]\!\right] \quad (4.b)$$

where, ρ is the air density, C_p stands for the power coefficient, η_{EM} is electrical/mechanical overall efficiency, L_{max} is the maximum hourly-averaged peak demand throughout the year and V_{min} is the minimum hourly-averaged wind speed throughout the whole year at a conservatively low hub elevation (in this study, $h_{hub,0} = 12\ m$) calculated using the logarithmic law.

In Equation 4.a the term $0.5\rho V_{min}^3 C_p \eta_{EM}$ is the wind turbine power per unit rotor area, πR_{WT}^2. It should be noted that R_{WT}^u obtained from Equation 4.a must not exceed the rotor radius of the largest available wind turbine. For instance, if we assume Vestas V164-8.0 is the largest available wind turbine, then R_{WT}^u is limited to 82m. In Equation 4.b, $[\![\cdots]\!]$ stands for rounding up to the nearest integer number. The denominator of the right-hand side of Equation 4.b is the maximum power that can be produced by the largest wind turbine available.

Since the rotor power coefficient depends on the wind speed, very conservative (low) value for the power coefficient is also assumed ($C_p = 0.2$). A conservative value for the combined efficiency of the electrical components and the gear train is also used $\eta_{EM} = 80\%$.

The upper limit for the PV panel area can be calculated by taking the same approach but based on daily-average data rather than hourly-averaged data. This is because the peak load might happen in hours that there is no sunlight and in practice PV panels always are accompanied by a storage component for standalone systems. The upper limit for the PV area, A_{PV}^u, can be found by:

$$A_{PV}^{u} = \frac{L_{d,max}}{I_{d,min}\eta_{PV}} \quad (5)$$

where, $L_{d,max}$ is the maximum daily-averaged demand throughout the year, $I_{d,min}$ is the minimum daily-averaged solar irradiance throughout the whole year, and η_{PV} is a conservative average value for the PV panel efficiency (for example 10%). The denominator of the right-hand side of Equation 5 is the PV power per unit area.

The upper size limit for the nominal power of the diesel generator is obtained based on the maximum hourly-averaged peak demand throughout the year L_{max} as follows:

$$P_{D,nom}^{u} = \frac{L_{max}(1+MOS)}{\eta_D} \quad (6)$$

where, $\eta_D = 0.4$, a conservative approximation for the diesel efficiency, and $(1 + MOS)$ is the load factor based on a margin of safety (MOS).

Adopting the same approach for the fuel cell, assuming a conservative approximate efficiency of $\eta_{FC} = 0.47$, the upper size limit for the nominal power of the fuel cell is obtained

$$P_{FC,nom}^{u} = \frac{L_{max}((1+MOS)}{\eta_{FC}} \quad (7)$$

The capacity of the electrolyser should be large enough to produce enough hydrogen for the fuel cell operation within one hour. Hence, the upper limit of the electrolyser size $P_{EL,nom}^{u}$ is associated to the upper limit of the fuel cell size $P_{FC,nom}^{u}$:

$$P_{EL,nom}^{u} = P_{FC,nom}^{u}/\eta_{EL} \quad (8)$$

where, the efficiency of the electrolyser in this study is taken as $\eta_{EL} = 0.74$.

The upper limit for the number of batteries in the battery bank, n_B^u is calculated based on the assumption that the battery bank can store enough energy to supply the demand load for an autonomy period $T_{a,B}$, normally taken as 1 day. Therefore, using the maximum daily-averaged demand load through the whole year, $L_{d,max}$, the upper limit for the number of batteries can be determined by:

$$n_B^u = \frac{T_{a,B}L_{d,max}(1+MoS)}{(1-SOC_{min})c_B V_B \eta_{B,d}} \quad (9)$$

where, $\eta_{B,d}$ is the battery efficiency in discharge, and SOC_{min} is the permissible minimum SOC without causing damage to the batteries, and $1 - SOC_{min}$ is the proportion of the battery bank capacity that can be used. In Equation 9, the nominator and denominator of the right-hand side are the required power to supply demand load for the autonomy period of $T_{a,B}$ with a margin of safety MoS and the extractable energy stored in a single fully charged battery in the battery bank respectively.

The general integrated configuration-size optimisation formulation above allows for formulation of special cases as well. There are cases that the designer wants to design a

specific configuration or fix the size of component prior to the optimisation. To do these the designer needs to use alternative upper and lower limits. By setting both the lower and upper limits of a component equal to zero, that component is excluded from the configuration. By doing so, the designer can fix the configuration. The formulation above also allows for pre-sizing of components. Pre-sizing refers to the selection of the size of a component outside the optimisation process. In order to exclude the size of a component from the set of design variables but keep the component in the HRES configuration the upper and lower limits are identical and set as the size of that component.

2.3 Design Qualities (Performance Measures)

In this study the following design qualities or performance measures are used in evaluating a HRES.

Unmet Load-Unmet load, the difference between the available power and the demand load, is the part of the demand load that is not supplied by the HRES. Using hourly averaged data, the unmet load U and the total annual unmet load U_t are defined as:

$$U = \begin{cases} L - P_a & if\ \ L > P_a \\ 0 & if\ \ L \leq P_a \end{cases} \tag{10}$$

and

$$U_t = \sum_{i=1}^{8760} U_i \tag{11}$$

where, L and P_a , respectively, are the hourly averaged demand load and available power from the system. For a system with wind, PV, battery, fuel cell and diesel, P_a is given by:

$$P_a = P_{WT} + P_{PV} + P_{B,e} + P_{FC,e} + P_{D,nom} \tag{12}$$

in which, P_{WT} and P_{PV} are the power produced by wind turbine(s) and PV panels, $P_{B,e}$ and $P_{FC,e}$ are the extractable power from the battery bank and fuel cell and $P_{D,nom}$ is the total nominal power of the diesel generator(s).

Wind power P_{WT} is given by:

$$P_{WT} = n_{WT}\frac{1}{2}\pi\rho {V_{hub}}^3 R_{WT}^2 C_p \eta_{EM} \tag{13}$$

In case the wind turbine to be used in the system is known, the rotor power coefficient C_p at various wind speeds, $C_p(V_{hub})$, is given in the turbine specification sheet and hence it is a known parameter. The same applies for η_{EM}. The hub hight h_{hub} is also a known parameter and using either of logarithmic or power laws V_{hub} is found readily.

In case the wind turbine is not selected/known prior to the optimisation process, model given in [20], or similar models, can be used for $C_p(V_{hub})$. For the overall wind turbine mechanical and electrical efficiency η_{EM}, a reasonable value (e.g. 90%) is used. In this case, the height of the hub depends on the size of the turbine, which is unknown at the start of the design phase. The following rule of thumb is used to estimate the hub height:

$$h_{hub} = \max\{h_c + R_{WT},\ 2R_{WT}\} \tag{14}$$

where, h_c is the minimum ground clearance for the blade tip.

Solar PV power P_{PV} is given by:

$$P_{PV} = IA_{PV}\eta_{PV} \quad (15)$$

where, I is the hourly averaged solar irradiance in W/m^2 , A_{PV} is the total area of the solar panels, and η_{PV} is the overall efficiency of the of the PV panels.

The extractable power from the battery bank $P_{B,e}$ is given by:

$$P_{B,e} = (SOC - SOC_{min})n_B c_B V_B \eta_B \quad (16)$$

where, c_B (Ah) and η_B stand for the unit nominal capacity and efficiency of batteries in discharge; n_B is the number of batteries in the bank; SOC is the state of charge of the battery bank, and SOC_{min} is the permissible minimum state of charge of the batter.

The extractable power from the hydrogen tank through a fuel cell, depends on the extractable mass of the hydrogen from the tank $M_{H_2,e}$ and the fuel cell efficiency η_{FC} and it is limited to the nominal power of fuel cell:

$$P_{FC,e} = min\{P_{FC,nom}, M_{H_2,e} m_{H_2} LHV \eta_{FC}\} \quad (17)$$

where, $m_{H_2} = 2.016 \times 10^{-3}\ kg/mol$ and $LHV = 33000$ Wh/kg are the molar mass and lower heating value of hydrogen, $P_{FC,nom}$ is the fuel cell nominal power and $M_{H_2,e}$, the extractable mass of hydrogen from hydrogen tank is the difference between the mass of stored hydrogen in the tank, M_{H_2} and $M_{H_2,min}$, the unextractable mass from the tank due to drop in the tank pressure:

$$M_{H_2,e} = M_{H_2} - M_{H_2,min} \quad (18)$$

Feed-in and Profit-In standalone systems the renewable power primarily supplies the demand load and, where applicable, if there is any excess power it is used to charge the battery bank and the hydrogen tank. Any excess power beyond this will be dumped. In grid connected systems, this excess power can be sold to the grid instead. The excess power that can be feed-in to the grid is given by:

$$P_{ex} = P_{WT} + P_{PV} - L - P_{B,c} - P_{EL,c} \quad (19)$$

where, $P_{B,c}$ and $P_{EL,c}$ are the power required to fully charge the battery bank and hydrogen tank respectively. $P_{B,c}$ is given by:

$$P_{B,c} = \frac{(1-SOC)n_B c_B V_B}{\eta_{B,c}} \quad (20)$$

where, $\eta_{B,c}$ is the battery charging efficiency, and $P_{EL,c}$ is given by:

$$P_{EL,c} = min\left\{P_{EL,nom}, \left(M_{H_2,max} - M_{H_2}\right)\frac{m_{H_2}LHV}{\eta_{EL}}\right\} \quad (21)$$

where, $P_{EL,nom}$ and η_{EL} are the electrolyser nominal power and its efficiency, and $M_{H_2,max}$ stands for the mass of the hydrogen in a fully charged hydrogen tank. The size of the hydrogen tank, $M_{H_2,max}$, can be calculated using the nominal power of the fuel cell and an autonomy period T_{a,H_2} (in days):

$$M_{H_2,max} = \frac{24P_{FC,nom}T_{a,H_2}}{LHV\eta_{FC}} \quad (22)$$

The total annual sellable excess power is given by:

.

$$feed = \sum_{i=1}^{8760} P_{ex,i} \quad (23)$$

Or alternatively, the actual annual profit can be calculated if the feed-in tariff t_{grid} is given. Since the feed-in tariff could have a variable rate depending on the time of the day (e.g. cheaper rate at off-pick hours), the profit can be calculated as:

$$profit = \sum_{i=1}^{8760}\left[P_{ex}t_{grid}\right]_i \quad (24)$$

Penetration-System penetration, p, is defined as the ratio of the annual renewable power to the annual demand load.

$$p = \frac{P_{R,t}}{L_t} = \frac{P_{WT,t}+P_{PV,t}}{L_t} \quad (25)$$

CO_2 Emission-The actual power produced by a diesel generator depends on its nominal power, the demand load/power deficit and the operational scenarios set in the energy management system. The hourly averaged diesel power P_D can get any value between 0 and $P_{D,nom}$. The total annual CO_2 emission (in kg) is given by [46]:

$$CO_2 = \frac{0.246\sum_{i=1}^{8760} P_{D,i}+0.08145P_{D,nom}T_D}{1000}\, e_l \quad (26)$$

where, T_D is the total number of hours of the operation per year, P_D is the hourly-averaged diesel power (in W) and e_l is the emission of CO_2 per litre of diesel consumption. This value depends on both the diesel generator and the fuel characteristics and normally has a value between $2.4 - 2.8\ kg/l$ range [46]. In this study, we assume $e_l = 2.68\ kg/l$.

Present Value of Total Life Span Cost (TLSC) - The present value of the system cost over its lifespan ($TLSC$) is given by [20]:

$$TLSC = \sum_{j=0}^{Ns}\frac{C_j}{(1+d)^j} \quad (27)$$

in which, d stands for the annual discount rate, Ns is the lifespan of the system and C_j is the cost in year j. The annual cost C_j includes the capital cost C_c for the year $j = 0$ of operation, the operation and maintenance costs $C_{O\&M}$ and the replacement cost C_r for the years $j =$

$1, \dots, N_S$ of operation. The capital cost of the system includes the initial cost C_i for buying the system components and their installation cost C_{inst}. The installation cost for each component is normally estimated as a fraction of the initial cost that component. The capital cost of the whole system is, the summation of the initial cost C_i and installation cost C_{inst}, is therefore given by:

$$C_c = \sum_{comp} C_{u,comp} S_{comp} (1 + \alpha_{inst,comp}) \quad (28)$$

in which, C_u and S are the unit cost and the size of component, and parameter α_{inst} is the fraction of the initial cost used for estimating the installation cost.

In cost analysis of HRES, only the cost of major components is considered and electronic and energy management system is excluded. There are two reasons behind this: (i) the cost of these components is much lower than the cost of other components and (ii) the cost of these components is almost independent of the size of the system, hence, in HRES size optimisation the inclusion or exclusion of these components does not affect the result of optimisation.

The operation and maintenance cost of the system $C_{O\&M}$ has two parts, namely, fixed $C_{O\&M,F}$ and variable $C_{O\&M,V}$ parts. Similar to installation cost the fixed part of O&M cost can be estimated as a fraction of the initial cost using parameter $\alpha_{O\&M}$. In HRES, the only variable part of O&M cost is the fuel cost, in case of having diesel generators in the system configuration. The overall O&M cost of HRES is therefore given by:

$$C_{O\&M} = \sum_{comp} \alpha_{O\&M,comp} C_{i,comp} + C_{O\&M,V,D} \quad (29)$$

where, $C_{O\&M,V,D}$ is the variable O&M cost of the diesel generator given by:

$$C_{O\&M,V,D} = \frac{0.246 \sum_{i=1}^{8760} P_{D_i} + 0.08145 P_{D,nom} T_D}{1000} C_{fuel} \quad (30)$$

in which, T_D, measured in hours, stands for total duration of operation of diesel generator annually, P_{D_i} is the hourly-averaged diesel power, and C_{fuel} is the fuel price.

Components with a lifespan shorter than the desired lifespan of the system need to be replaced throughout the duration of the system operation. The replacement cost of a component $C_{r,comp}$ depends on the number of replacements $n_{r,comp}$ during the lifespan of the system and the capital cost of that component $C_{c,comp}$. The overall replacement cost of a HRES is therefore given by:

$$C_r = \sum_{comp} n_{r,comp} C_{c,comp} \quad (31)$$

The number of replacements of PV panels and wind turbines and are calculated based on their nominal lifespan using the following equation:

$$n_{r,comp} = \left\lceil \frac{N_S}{N_{nom,comp}} \right\rceil \quad (32)$$

where, $N_{nom,comp}$ is the nominal lifespan of PV panel $N_{nom,PV}$ or wind turbine $N_{nom,WT}$. Both of them, similar to the system lifespan N_S, are measured in years.

The number of replacements of fuel cell, electrolyser and diesel generator are calculated based on the actual usage of these components and is given by:

$$n_{r,comp} = \left\lceil \frac{N_S T_{comp}}{N_{comp,nom}} \right\rceil \quad (33)$$

where $N_{comp,nom}$ and T_{comp} are, respectively, the nominal lifespan and the operating time, both in hours.

The number of replacements for batteries, $n_{r,B}$, is calculated using the nominal lifespan of the batteries and the equivalent life of the battery in years, whichever is shorter as given by [20]:

$$n_{r,B} = \left\lceil \max \left\{ \frac{N_S}{N_{nom,B}}, \frac{N_S}{N_{eq,B}} \right\} \right\rceil \quad (34)$$

where, $N_{eq,B}$ stands for the equivalent life of the battery and $N_{nom,B}$ is the nominal life of the battery, both measured in years. The nominal life of lead-acid batteries is about 4 years. The equivalent life of the battery depends on the number and depth of charge-discharge cycles, as given by:

$$N_{eq,B} = \frac{1}{\sum_{k=1}^{n_d} \frac{1}{\left\lceil n_{cycle\ to\ fail} \right\rceil_k}} \quad (35)$$

where, n_d is the total number of charge-discharge cycles per year, and $\left\lceil n_{cycle\ to\ fail} \right\rceil_k$, the number of cycles to failure, for lead-acid batteries is given by [20] as a function of depth of discharge DOD:

$$\left\lceil n_{cycle\ to\ fail} \right\rceil_k = 540.1 DOD_k^{-0.991} \quad (36)$$

Table 1 summarises the value of cost modelling parameters required for cost analysis of HRES as reported in [46, 50, 51].

Table 1-Cost modelling parameters used in this study

	Wind turbine	PV panel	Battery	Diesel generator	Fuel cell	Electrolyser
S	Rotor area $A_{WT}\ (m^2)$	Panel area $A_{PV}\ (m^2)$	Battery bank capacity (Ah)	Nominal power$P_{D,nom}\ (W)$	Nominal power $P_{FC,nom}\ (W)$	Nominal power $P_{EL,nom}\ (W)$
C_u	Eq. 37	Eq. 38	Eq. 39	Eq. 40	$4.08\$/W_{nom}$	$2\$/W_{nom}$
α_{inst}	0.2	0.4	0	0	0	0
$\alpha_{O\&M}$	0.03	0.01	0.01	0.15	0.1	0.1
N_{nom}	25 years	20 years	4 years	10,000 hours	5,000 hours	60,000 hours

For wind turbine:

$$C_u(\$/m^2) = \begin{cases} 480 & A_{WT} > 1180\ m^2 \\ -207 \times log(A_{WT}) + 1944 & A_{WT} \leq 1180\ m^2 \end{cases} \quad (37)$$

For PV panel:

$$C_u(\$/m^2) = \begin{cases} 220 & A_{PV} > 1000\ m^2 \\ -51.64 \times log(A_{PV}) + 580 & A_{PV} \leq 1000\ m^2 \end{cases} \quad (38)$$

For battery bank, the unit cost depends on the battery capacity, c_B, and a discount rate for bulk purchase:

$$C_u(\$/Ah) = 163 c_B^{-1.14} \times \begin{cases} 0.8 & n_B > 100 \\ -0.0015 n_B + 0.95 & n_B \leq 100 \end{cases} \quad (39)$$

For diesel generator:

$$C_u(\$/W) = \begin{cases} 0.4 & P_{D,nom} > 50000\ W \\ 1.7 \times 10^{-10} P_{D,nom}^2 - 1.84 \times 10^{-5} P_{D,nom} + 0.8971 & P_{D,nom} \leq 50000\ W \end{cases} \quad (40)$$

Levelised Cost of Energy-Levelised cost of energy is calculated based on the usable power produced by the system and the cost of production within a year. The annualised cost of the system, C_a, is determined by:

$$C_a = TLSC \frac{d(1+d)^{N_s}}{(1+d)^{N_s}-1} \quad (41)$$

where, the fraction in this equation is the uniform capital recovery factor. For standalone HRES, the LCE of a system, C_l is given by:

$$C_l = \frac{C_a}{P_t} \quad (42)$$

where, P_t is the annual usable power output of the system. It should be noted that for standalone HRES the output power is not necessarily entirely usable. The produced power excess to the load is used for charging the battery bank and hydrogen tank. However, if the excess power is more than the required power for charging the battery bank and hydrogen tank, the difference will be dumped. Hence, the usable annual output for standalone HRES is:

$$P_t = L_t - U_t \quad (43)$$

in which, L_t and U_t are the total annual demand load and the total annual unmet load respectively.

For on-grid HRES, the unmet load is compensated by the grid. Therefore, the LCE has two terms, namely the cost of producing energy by the HRES and the cost of buying electricity from the grid to compensate for the unmet load:

$$C_l = \frac{C_a}{P_t} + \frac{C_{u,t}}{P_{u,t}} \quad (44)$$

The cost of electricity from grid depends on the unmet load and, in the case of variable rates, the time of the day. The total cost of electricity from the grid is therefore given by:

$$C_{u,t} = \sum_{i=1}^{8760} \left[P_u C_{grid} \right]_i \quad (45)$$

2.4 Optimisation Formulation

In view of the design variables and design qualities defined in the previous two subsections, the optimisation problem can be formulated as:

$$min\, \vec{Y}_1(\vec{X}) \text{ and } max\, \vec{Y}_2(\vec{X}) \quad (46.a)$$

$$s.t.$$

$$\vec{Y}_3 \leq \vec{Y}_{3,c} \quad (46.b)$$

$$\vec{Y}_4 \geq \vec{Y}_{4,c} \quad (46.c)$$

$$\vec{X}^l \leq \vec{X} \leq \vec{X}^u \quad (46.d)$$

where, $\vec{X} = \{n_{WT}, A_{WT}, A_{PV}, n_B, P_{D,nom}, P_{FC,nom}, P_{EL,nom}\}$ is the vector of design variables, with $\vec{X}^l$ and $\vec{X}^u$ as given by Equations 2 through 9 for the generic configuration, or as explained above for special cases of retrofitting, fixed configuration and pre-sized components. Vectors $\vec{Y}_1$ and $\vec{Y}_2$, respectively, contain the objectives to be minimised and maximised. Vectors $\vec{Y}_3$ and $\vec{Y}_4$ contains those design qualities which are subjected to the constraints $\vec{Y}_{3,c}$ and $\vec{Y}_{4,c}$.

These four vectors are disjoint subsets of design qualities:

$$\vec{Y}_1 \cup \vec{Y}_2 \cup \vec{Y}_3 \cup \vec{Y}_4 \subseteq \{TLSC, LCE, U_t, CO_2, p, feed, profit\} \quad (47.a)$$

$$\vec{Y}_1 \cup \vec{Y}_3 \subseteq \{TLSC, LCE, U_t, CO_2\} \quad (47.b)$$

$$\vec{Y}_2 \cup \vec{Y}_4 \subseteq \{p, feed, profit\} \quad (47.c)$$

3 Optimisation Method

The optimisation methods must be able to search the design space at two levels, namely, configuration level and size level. In this study, we use a GA and a nondominated sorting GA (NSGA-II) for single and multiobjective optimisation respectively. The integrated configuration-size formulation and the single and multiobjective optimisation algorithms have been implemented in the software tool MOHRES (Multiobjective Optimisation of Hybrid Renewable Energy Systems) [52, 53]. Figure 1 shows the dataflow in MOHRES.

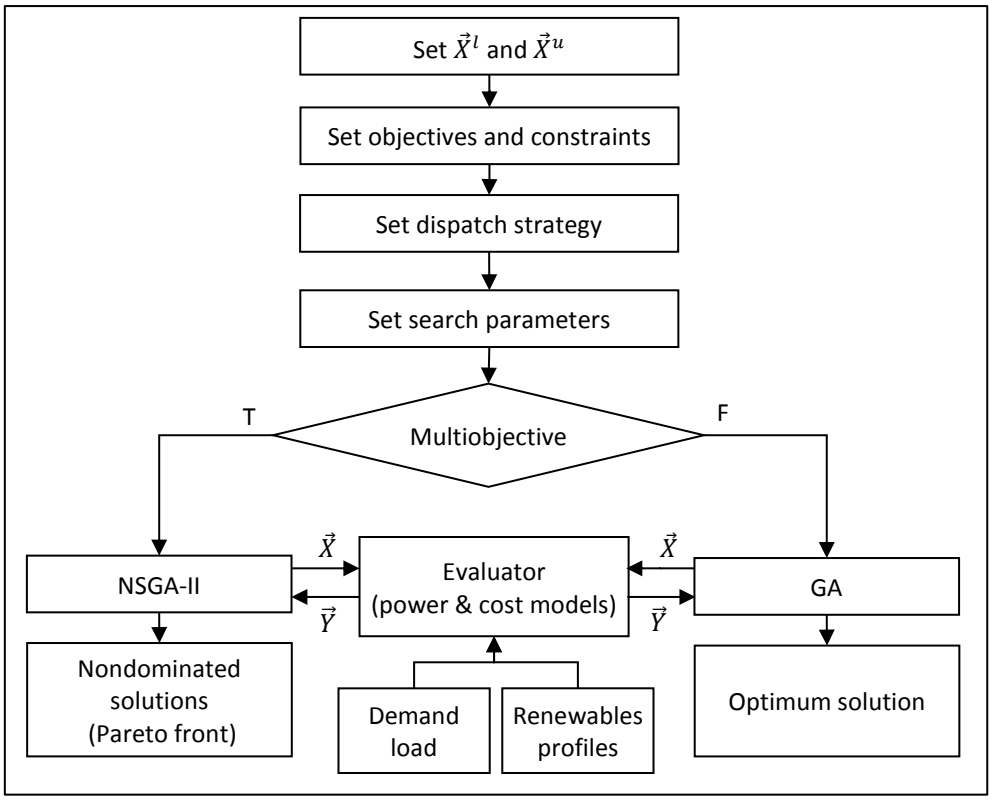

Figure 1-Interated configuration-size optimisation dataflow in MOHRES

The upper and lower limits of the design variables are set using Equations 2-9 for a full integrated configuration-size optimisation, and a combination of these equations and fixed values for special cases of optimisation for retrofitting and fixed configuration. Objectives and constraints are set according to the optimisation problem 46 and 47.

In configurations which include more than one storage/auxiliary component different dispatch strategies can be defined. A dispatch strategy is defined based on the charging and usage orders of the storage/auxiliary components. For instance, in a wind-PV-fuel cell-electrolyser-diesel-battery bank configuration, 6 different usage orders can be defined based on the precedence of the battery bank, diesel generator and fuel cell in compensating the power deficit. For the same configuration, 2 charging orders can be defined based on the precedence of the battery bank and hydrogen tank in charging where there is an excess power [26].

Generally speaking, a search mechanism should be able to deliver both exploration and exploitation at all levels. However, here at the configuration level we are dealing with a highly discrete and small design space (of around twenty-odd members for the problem at hand). Therefore, exploitation does not apply at configuration level. The reproduction operators, crossover and mutation, therefore must be designed in such a way that collectively provide exploration and exploitation at size level and exploration at configuration level.

Arithmetic weighted crossover is a natural choice for crossover mechanism in sizing problems. A weighted arithmetic crossover is therefore used for exploitation of the design space at size level. Each crossover operation generates two offspring as defined by:

$$\vec{X}_{child,1} = \lambda \vec{X}_{parent,1} + (1-\lambda)\vec{X}_{parent,2} \quad (48.a)$$

$$\vec{X}_{child,2} = \lambda \vec{X}_{parent,2} + (1-\lambda)\vec{X}_{parent,1} \quad (48.b)$$

where, $\lambda \in (0,1)$ is a random number.

The arithmetic crossover mechanism defined above, has some exploration capability at the configuration level: by combining two parents of different configurations (combining of two chromosomes with some zero genes placed at different locations), there is a chance that the offspring have a configuration with more components (a chromosome with more non-zero genes) than those of its parents. For example, a crossover between a wind-PV solution and a PV-battery-diesel solution will lead to at least one wind-PV-battery-diesel solution (depending on the value of the random number λ in Equations 48). The exploration at configuration level due to arithmetic crossover is a one-way 'upward' exploration. That is, it can only produce offspring with similar or more populated configurations than those of parents. An upward/downward change in configuration refers to adding/removing components to/from the system configuration.

The mutation operator is therefore designed in such a way that besides exploration at size level, conduct a 'downward' exploration at configuration level too. At configuration level, a number of randomly selected genes in a randomly selected solution are set to zero. This is equivalent to removing the corresponding components from the configuration (downward exploration). Mutation at configuration level operates as:

$$\vec{X}_{mute} = \vec{M}_1 \circ \vec{X}_{parent} \quad (49)$$

where, $\vec{M}_1$ is a $1 \times n_x$ mask vector with randomly generated 0 and 1entries, the operator '$\circ$' is Hadamard (entry-wise) product and n_x is the number of design variables in the chromosome (here 7). As a result of the mutation operation above, the design variables corresponding to the zero elements of the mask vector $\vec{M}_1$ are set to zero. This is equivalent to the exclusion of the corresponding components from the configuration and therefore a downward exploration in the configuration.

At size level, a dynamic mutation operator is designed with two functions of exploration at earlier generations and exploitation at later generations. Although it is very unusual to use mutation operator for exploitation, it is shown later that adding exploitatory functionality to the mutation operator will boost the performance of the search significantly. A selected solution is perturbed according to:

$$\vec{X}_{mute} = \vec{X}_{parent} + \delta\vec{X} \quad (50)$$

where, the perturbation vector $\delta\vec{X}$ is a randomly generated vector in the neighbourhood of the parent. The radius of the neighbourhood shrinks with a factor of $\left(1 - \frac{i_{gen}-1}{n_{gen}-1}\right)$, in which, n_{gen} is the total number of generations and i_{gen} $(1 \le i_{gen} \le n_{gen})$ is the current generation number. This allows fine-tuning (exploitation) at higher generations.

The $i-th$ element of the perturbation vector $\delta\vec{X}$, δX_i, is a random value selected from the $i-th$ row of the neighbourhood matrix N_{mute} defined as:

$$N_{mute} = M_2 \circ I_{mute} \quad (51)$$

in which, M_2 is an $n_x \times 2$ mask matrix with randomly generated 0 and 1entries and I_{mute} is the shrinking mutation neighbourhood:

$$[I_{mute}]_{n_x \times 2} = \left(1 - \frac{i_{gen}-1}{N_{gen}-1}\right) \begin{bmatrix} \vec{X}^l - \vec{X}_{parent} \\ \vec{X}^u - \vec{X}_{parent} \end{bmatrix}^T \quad (52)$$

The mask matrix M_2 is responsible for selecting the genes going through mutation at size level and the direction of the perturbation. For instance, a randomly generated matrix $M_2 = \begin{bmatrix} 0 & 0 & 1 & 1 & 0 & 1 & 0 \\ 0 & 1 & 1 & 0 & 0 & 0 & 0 \end{bmatrix}^T$ excludes X_1 , X_5 and X_7 (the number of wind turbines, and the size of diesel generator and electrolyser) from mutation (no perturbation for these design variables), allows a positive perturbation for X_2 (the size of wind turbine), a positive or negative perturbation for X_3 (the size of PV panels), and a negative perturbation for X_4 and X_6 (the size of battery bank and fuel cell).

While the parent selection for the mutation at configuration level takes place randomly, the parent selection at the size level is based on a combination of a random selection and a fitness-based selection. The classical random selection is used where the population is diverse. The parent selection will be switched to a fitness based, where a roulette wheel is used to give higher chance of fine-tuning to the fitter solutions, as the diversity of the population decreases towards the end of the search (where the average fitness fit_{av} approaches the maximum fitness fit_{max}). In this study the limit of $\frac{fit_{av}}{fit_{max}} \geq 0.9$ is used as the limit for fine-tuning (switching the parent selection from random to roulette wheel based).

Another uncommon feature of the mutation operator designed for the problem at hand is related to the probability of mutation P_m. A dynamic P_m is defined as follows:

$$P_m = P_{m,config} + P_{m,size} \quad (53)$$

where, P_m, $P_{m,config}$ and $P_{m,size}$, respectively, represent the total mutation rate, the fraction of the mutations applied at the configuration level (Equation 49), and the fraction of the mutations applied at the size level (Equation 50):

$$P_{m,config} = 0.5P_{m,0}\left(1 - \frac{i_{gen}-1}{n_{gen}-1}\right) \quad (54)$$

$$P_{m,size} = 0.5P_{m,0} \quad (55)$$

The total mutation rate P_m ($0.5P_{m,0} \leq P_m \leq P_{m,0}$) decreases as the generation number i_{gen} increases. The limits $P_{m,0}$ and $0.5P_{m,0}$ are associated to $i_{gen} = 1$ and $i_{gen} = n_{gen}$ respectively. A relatively high value for $P_{m,0} \sim 0.5 - 0.9$ should be used in order to allow effective mutation operation at both size and configuration levels.

It should be noted that, although the design variables are treated as continuous real numbers, for practicality reasons, the design variables are rounded. A_{PV} and n_B are rounded up to the

nearest integer number, the nominal powers (diesel, fuel cell and electrolyser) are rounded up to the nearest 100 watt, and the wind turbine rotor radius R_{WT} is rounded up to the nearest 10 cm.

In the problem formulation of (46) and (47) above, there is no limitation on the number of constraints. Hence, the initial population generation for highly constrained optimisation problems may take a very long time if infeasible solutions are rejected. In such cases, the crossover and mutation may also become ineffective due to generating solutions with high chance of being rejected due to infeasibility. Hence, penalising infeasible solutions is the best approach in these cases. On the other hand, for flexible design spaces, adopting a rejection method leads to starting from a feasible set of solutions which is more likely to get to the global optima in a smaller number of generations. Therefore, two methods of rejection and penalising infeasible solutions are used for different cases, depending on the number of constraints and the rigidity of the design space.

Equation 56 shows a generalised fitness function with a great flexibility, which is developed for single objective optimisation using GA. This form can be used for both maximisation and minimisation cases and can take the form of a raw fitness as well as the form of a penalised fitness, by setting some coefficients by the user.

$$fit = (fit_r \prod_{i=1}^{n_c} P_i)(1 - fit_0) + fit_0 \quad (56)$$

In this equation, fit stands for the fitness, fit_r is the normalised raw fitness, n_c is the number of constraints, fit_0 is the worst possible normalised fitness (set by the designer), and $0 < P_i \leq 1$ is the penalty value for the i-th constraints. A value of $fit_0 = 0.1$ is used for the single objective optimisation cases studies in this paper. By doing this, we prevent assigning very small fitness values to bad solutions, and therefore, any potentially good information from the worst solution can still be retrieved in crossover operation.

The raw fitness for a solution is calculated as follows:

$$fit_r = \begin{cases} \frac{f_n}{f+f_n} & \text{when } f \text{ is to be minimised} \\ \frac{f}{2f_n} & \text{when } f \text{ is to be maximised} \end{cases} \quad (57)$$

where f is the calculated objective function for that solution, and f_n, the average value of the objective function of solutions in the initial population, is used to normalise the fitness.

Here, the infeasibility is measured in terms of both the number of contradicted constraints and the amount of deviation from the constraint limits. The penalty applied to each contradicted constraint is calculated by:

$$P_i = \exp(-\mu_i \delta_i) \quad (58)$$

where, δ_i is the deviation from the constraint limit and $0 \leq \mu_i$ is the strength of the applied penalty on the constraint i. Parameter $\mu_i = 0$ represents the case of no penalty if the constraint i is contradicted. Deviations δ_i are normalised values and given by:

$$\delta_i = \begin{cases} 0 & satisfied\ inequality\ constraint \\ \left|\frac{Y_i - Y_{c,i}}{\max\{Y_{c,i}, Y_i\}}\right| & contradicted\ inequality\ constraint \end{cases} \quad (59)$$

where, Y_i's are the entries of $\vec{Y}_3 \cup \vec{Y}_4$ and $Y_{i,c}$'s are the entries of $\vec{Y}_{3,c} \cup \vec{Y}_{4,c}$ as defined in the optimisation problem of (46) and (47). The normalisation term $\max\{Y_{c,i}, Y_i\}$ is always nonzero for any contradicted constraint, irrespective of the type of inequality constraint and the values $Y_{c,i}$ and Y_i.

The goal of NSGA-II (nondominated sorting genetic algorithm) is to find the best estimation of the Pareto front solutions. This is done by generating a set of nondominated solutions and moving it forward towards the actual Pareto front generation by generation. A successful NSGA-II should be aiming at producing enough and uniformly distributed solutions on the Pareto front. In order to improve the first front generation by generation, the same reproduction operators (crossover and mutation) as those defined for single objective GA can be used. In single objective GA, the parent selection for crossover is solely based on a roulette wheel, which is formed based on the fitness of the solutions in the population. In multiobjective NSGA-II, the parent selection for crossover is different. It is based on a tournament selection mechanism which is based on (i) the rank of a solution (the front that the solution belongs to) and (ii) the crowding distance. The crowding distance is a measure of how close a solution is to its neighbours on the same front. Both are important qualities. The rank of a solution is important as solutions on the low-rank fronts are more likely to produce better offspring, if selected as a parent. The crowding distance is also important as those solutions located in less crowded regions, if selected as a parent for crossover, are more likely to produce offspring in their own neighbourhood and therefore filling the gaps on the front.

The common search parameters for both GA and NSGA-II are: P_c, $P_{m,0}$, n_{pop} and n_{gen}. For GA, the method of handling of infeasible solutions (rejection or penalty) is also a search parameter, and so are the penalty weights μ_i in case of using penalty method. For any generated design candidate within the GA or NSGA-II search (produced either randomly as in initial population generation or as a result of the mutation and crossover using Equations 48-55), the evaluator takes the system size $\vec{X}$, the demand load and renewables profiles and uses the power and cost models (Equations 10-45) to find the relevant qualities of the design candidate $\vec{Y}$ (objectives and constrained design qualities as defined in 47). These $\vec{Y}$ values are returned to the search algorithm for assigning fitness and rank for that individual according to Equations 56-59.

4 Case Studies

In this section, 8 case studies, denoted by CS1 to CS8, are reported. These case studies are designed carefully to assess the robustness of the presented problem formulation in solving different types of HRES optimisation problems and to evaluate the performance of the developed GA and NSGA-II for integrated configuration-size optimisation.

Case studies are summarised in Table 2. The first six case studies are single objective and the last two are multiobjective. Three sites are used for these case studies. The hourly averaged demand load and the renewable resources for four seasonal typical days of Site 1 are given in the appendix. Site 2 has similar demand load profile as that of Site 1 but the solar irradiance and wind speed are, respectively, 20% lower and 50% higher than of those in Site 1. Site 3 is a low-renewable site. The demand load and wind profiles are identical to Site 1, but the solar

irradiance is half of that of Site 1. Both standalone (S) and grid connected cases (G) are considered.

The purpose of CS1 is to show how the presented problem formulation starts with a generic all-components-in configuration and ends with an optimum configuration by eliminating cost intensive components. The optimisation problem of CS2 is identical to that of CS1 but the renewable resource profile is different. This case study is planned to show how the integrated configuration-size optimisation problem formulation finds a different optimum configuration as the renewable resources' profiles change. CS3 is defined to show how adding a new constraint influences the optimum configuration. In CS4 the optimum size of components for a predefined configuration are obtained. This case study is planned to show the flexibility of the problem formulation in dealing with fixed configurations (reducing from integrated configuration-size optimisation to size optimisation only). CS5 and CS6 are aimed at showing the flexibility of the formulation in delivering special cases of retrofitting of an existing power system by adding new components to an existing system. In CS5, the existing power system is a $5\ kW\ (nominal)$ diesel generator. This diesel generator produces 37 tonnes of CO_2 emission per year when operating continuously. The purpose of the optimisation is to find the best retrofitted configuration that includes this diesel generator (for saving) but reduces its CO_2 emission to less than 500 kg per year (for environment). CS6 presents another retrofitting case but starts with a different existing power system (a $30kW\ @V_{rated} = 9\ m/s$ wind turbine with a rotor radius of 6.9 m) and aims at a fixed retrofitted configuration (wind-PV-battery). The intention for this retrofitting is to invest in renewable energy by selling the excess power to the grid.

Table 2-Summary of Case Studies

Case study	Configuration	Obj.	Const.	Site	Standalone/ on grid
CS1	Generic; $\vec{X}^l$ Eq. 2; $\vec{X}^u$ Eq.s 3 to 9	LCE	$U_t = 0$	1	S
CS2	Generic; $\vec{X}^l$ Eq. 2; $\vec{X}^u$ Eq.s 3 to 9	LCE	$U_t = 0$	2	S
CS3	Generic; $\vec{X}^l$ Eq. 2; $\vec{X}^u$ Eq.s 3 to 9	LCE	$U_t = 0$ $p > 200\%$	2	S
CS4	Fixed: W-FC-EL $\vec{X}^l$ Eq. 2 ; $\vec{X}^u = \{R^u_{WT}, 0, 0, 0, P^u_{FC,nom}, P^u_{EL,nom}\}$ & Eq.s 4, 7 and 8	LCE	$U_t = 0$	1	S
CS5	Retrofitting: diesel only to generic config. $\vec{X}^l = \{0,0,0, P_{D,nom}, 0,0\}$ $\vec{X}^u = \{R^u_{WT}, A^u_{PV}, n^u_B, P_{D,nom}, P^u_{FC,nom}, P^u_{EL,nom}\}$ & Eq.s 4, 5 and 7 through 9 $P_{D,nom} = 5kW$	$TLSC$	$U_t = 0$ $CO_2 < 500\ kg$	1	S
CS6	Retrofitting: wind only to fixed config. W-PV-B $\vec{X}^l = \{R_{WT}, 0,0,0,0,0\}$ $\vec{X}^u = \{R_{WT}, A^u_{PV}, n^u_B, 0,0,0\}$ & Eq.s 5 and 9 $R_{WT} = 6.9\ m$	$profit$	$U_t = 0$ $TLSC \leq 250,000$	1	G
CS7	Generic; $\vec{X}^l$ Eq. 2; $\vec{X}^u$ Eq.s 3 to 9	LCE U_t	$p \geq 60\%$	1	S
CS8	Generic; $\vec{X}^l$ Eq. 2; $\vec{X}^u$ Eq.s 3 to 9	LCE U_t CO_2		3	S

In single objective optimisation problems, we are looking for a solution with best performance in terms of one of the design qualities and have 'hard' constraints on some other design qualities. For instance, in CS1 we are looking for the cheapest fully reliable system (min LCE subject to $U_t = 0$). From a practical point of view, this is not always the case. We can often tolerate some inferior performance measures as we know that losing on one quality leads to a gain on another quality (conflicting objectives). In cases like this conducting a multiobjective optimisation is the best way to get an insight to the interaction between different objectives. Once a Pareto front is obtained the designer selects a solution through a trade-off study. Case studies CS7 and CS8 are multiobjective problems. In CS7 we deal with two conflicting cost-related and reliability-related objectives: LCE and U_t. CS8 is defined for a low-renewables site with three conflicting objectives: LCE, U_t and the third one related to the impact of the system on the environment: CO_2 emission.

In all case studies the usage order is defined as: battery first, then fuel cell (hydrogen), and then diesel. The charging order is defined as: battery first then hydrogen tank. All power and cost model parameters which have not been defined within the text are given in Table A1 in the appendix.

For consistency the same set of search parameters: $P_c = 0.3$, $P_{m,0} = 0.9$ and $n_{gen} = 100$ are used for both single objective and multiobjective cases. Population size n_{pop} is set to 20 and 40 for GA and NSGA-II respectively.

4.1 Results and Discussion

The optimum solutions for the first six case studies are summarised in Table 3, followed by detailed discussion including the performance of the GA for each case study.

Table 3-Optimum solutions for single objective case studies CS1 through CS6

Case study	$\vec{X}_{opt}$							$\vec{Y}_{opt}$					
	n_{WT}	R_{WT} (m^2)	A_{PV} (m^2)	n_B	$P_{D,nom}$ (W)	$P_{FC,nom}$ (W)	$P_{EL,nom}$ (W)	$TLSC$ (1000\$)	LCE (c/kWh)	U_t (kW)	p (%)	CO_2 (kg)	$profit/feed$ (1000\$/MW)
CS1	1	0	296	232	0	0	0	186	23.0	0	139	0	N/A
CS2	1	4.7	0	14	8300	0	0	186	23.1	0	134	5700	N/A
CS3	1	5.7	14	62	0	0	0	192	23.9	0	201	0	N/A
CS4	1	11.6	0	0	0	8500	4800	694	86.2	0	378	0	N/A
CS5	1	0	285	232	5000	0	0	192*	23.8*	0	134	400	N/A
CS6	1	6.9	372	112	0	0	0	250**	31.0**	0	284	0	(12.8/106.7)

*Excluding the capital cost of the diesel generator
**Excluding the capital cost of the wind turbine

CS1: Configuration-size optimisation-Site 1

A closer look at the renewable resources of the appendix suggests that this site has low-wind and high-solar irradiance profiles. In view of this, although starting from a generic wind-PV-battery-diesel-Fuel cell/electrolyser, a PV-battery configuration is the optimum configuration that we expect to see as a result of an integrated configuration-size optimisation for CS1. Staring from a generic configuration and ending with a PV-battery configuration implies that wind turbine, diesel generator and fuel cell/electrolyser have been removed from the configuration at some points during the search process. Figure 2 shows the GA search history for this case study and Table 4 shows the configuration and components' size of the best solution in each generation. The last column of Table 4 shows the change in the

configuration, where, as mentioned before downward and upward directions stand for removing and adding components to the system respectively.

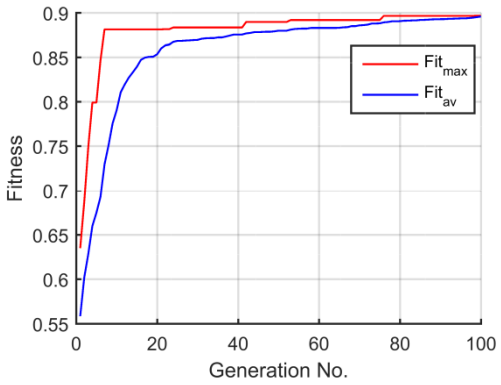

Figure 2-GA search history for CS1

The final configuration is due to a combination of a number of downward and upward changes as shown in Table 4. The best solution of the second generation ($i_{gen} = 2$), is the result of a downward mutation of one of the solutions in the first generation, which has led to the removal of the fuel cell (or electrolyser) and consequently the accompanied electrolyser (fuel cell). A further downward mutation leads to the removal of the wind turbine and diesel at $i_{gen} = 6$. An upward mutation or crossover brings back the diesel generator into the configuration at $i_{gen} = 76$, which is removed again later as a result of another downward mutation at $i_{gen} = 99$. Having both downward and upward changes in the configuration proves the capability of the developed algorithm in exploring various configurations while optimising the size of components. Exploration at configuration level at both directions shows that the algorithm does not get trapped in a local optima.

Table 4- System configuration in the search history of CS1

i_{gen}	fit_{max}	fit_{av}	R_{WT} (m^2)	A_{PV} (m^2)	n_B	$P_{D,nom}$ (W)	$P_{FC,nom}$ (W)	$P_{EL,nom}$ (W)	Direction of change in configuration
1	0.6352	0.5586	2	339	278	43400	47900	52000	no change
2	0.6876	0.6021	10.9	122	772	32300	0	0	downward
3	0.7494	0.6288	8	219	734	12800	0	0	no change
4	0.7992	0.6602	4.5	422	552	6100	0	0	no change
5	0.7992	0.6751	4.5	422	552	6100	0	0	no change
6	0.8465	0.6929	0	314	832	0	0	0	downward
7	0.8815	0.7293	0	356	282	0	0	0	no change
…									no change
75	0.8920	0.8883	0	323	236	0	0	0	no change
76	0.8967	0.8894	0	297	234	100	0	0	upward
…									no change
98	0.8967	0.8947	0	297	232	100	0	0	no change
99	0.8968	0.8953	0	296	232	0	0	0	downward
100	0.8968	0.8960	0	296	232	0	0	0	no change

With reference to Table 4, one can observe that in earlier generations, changes in configuration leads to jumps in fit_{max}. However, in later generations changes in configuration are more like fine-tuning of configuration (i.e. adding a very small diesel of 100 W to the system at $i_{gen} = 76$ and then removing it at $i_{gen} = 99$) and have smaller effect on maximum fitness.

For this particular case study, in which the optimum solution includes only two components in the configuration, we can prove the optimality of the obtained sizes by employing a refined exhaustive search in the neighbourhood of the solution. Using a grid size of 1 for both A_{PV} and n_B, within the limits: $200 \leq A_{PV} \leq 400$ and $150 \leq n_B \leq 350$, over 40000 system analyses are required. The results are shown in Figure 3. The solution identified by red circle has the minimum LCE while satisfying the constraint of $U_t = 0$. This is identical to the optimum solution obtained by the GA ($A_{PV} = 396\ m^2; n_B = 232$).

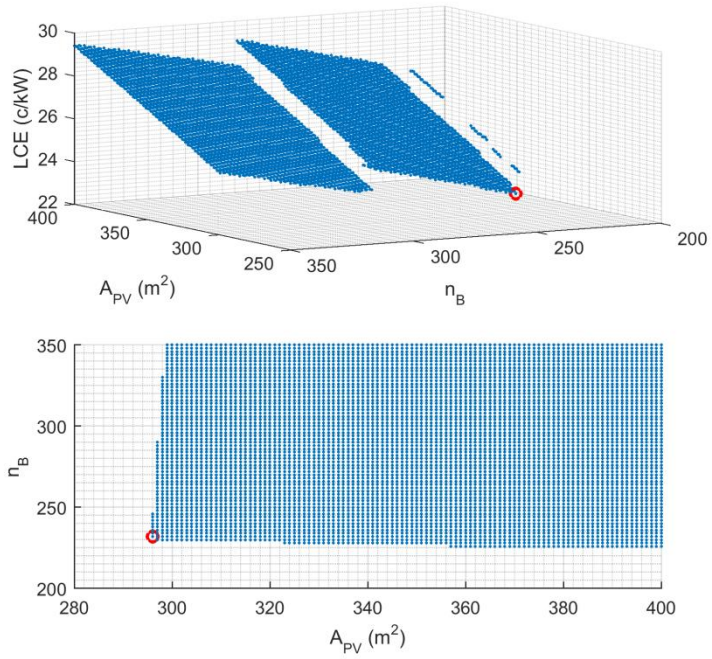

Figure 3-Exhuastive search results; top: feasible solutions; bottom: feasible design space

It should be noted that, although for this case study the optimality of the PV-battery configuration could be argued with confidence with reference to the renewable resource profiles, there is no practical means to prove it. If we were to use an exhaustive search, even by assuming a very course grid of only 100 points for every one of the six design variables, 10^{12} system evaluations over the entire of the domain would be required.

CS2: Configuration-size optimisation -Site 2

In comparison to the renewable resources of CS1, in CS2 the wind is 50% stronger but the solar irradiance is 20% weaker. This makes, wind energy more cost effective and solar energy more cost intensive. Therefore, compared to the optimum configuration of CS1, we expect to see an increase in the share of power production by wind and a reduction of the contribution of PV. In fact, in this case study, the PV has been eliminated from the generic configuration. The presence of diesel in the configuration can be explained in view of the fact that, unless the site has high renewable resource profiles, with the current prices (the cost parameters used in this study) the LCE produced by diesel generator is still less than the LCE produced by renewables. Figure 4 shows the GA search history for this case study and Table 5 shows the configuration history. This table shows a number of bidirectional changes in the configuration ($i_{gen} = 2$, 4, 8 and 16) as well as downward and upward changes ($i_{gen} = 21$, 35 and 36). For instance the configuration of $i_{gen} = 21$ has simultaneously gone through a downward mutation, which has led to the removal of the wind turbine, and an upward

mutation or crossover which has brought back the diesel into the configuration. A closer look at the configurations obtained by bidirectional changes, one can see that bidirectional changes correspond to the removal/adding of a renewable component and adding/removal of a storage component.

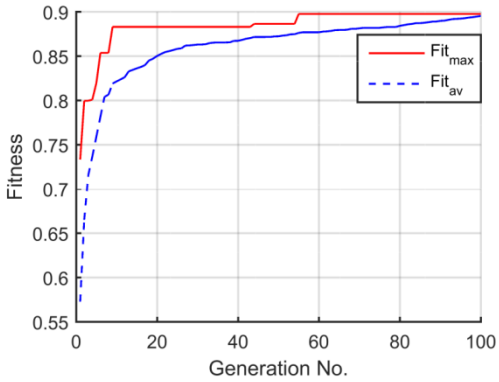

Figure 4-GA search history for CS2

Table 5- System configuration in the search history of CS2

i_{gen}	fit_{max}	fit_{av}	R_{WT} (m^2)	A_{PV} (m^2)	n_B	$P_{D,nom}$ (W)	$P_{FC,nom}$ (W)	$P_{EL,nom}$ (W)	Direction of change in configuration
1	0.681	0.557	3.1	460	446	93600	15900	14600	no change
2	0.756	0.597	5.6	349	56	102800	0	0	downward
3	0.756	0.633	5.6	349	56	102800	0	0	no change
4	0.790	0.681	0	459	260	102800	0	0	downward
…									no change
7	0.813	0.730	0	402	236	80400	0	0	no change
8	0.832	0.749	4.2	277	80	13000	0	0	upward
…									no change
15	0.832	0.802	4.2	277	80	13000	0	0	no change
16	0.835	0.807	6	21	418	0	0	0	downward
…									no change
20	0.835	0.814	6	21	418	0	0	0	no change
21	0.845	0.821	0	385	220	1300	0	0	downward and upward
…									no change
34	0.845	0.834	0	385	220	1300	0	0	no change
35	0.850	0.836	2.3	349	288	0	0	0	downward and upward
…									no change
38	0.850	0.838	2.3	349	288	0	0	0	no change
39	0.854	0.839	5.3	0	150	5800	0	0	downward and upward
…									no change
100	0.881	0.874	4.7	0	14	8300	0	0	no change

CS3: Configuration-size optimisation - high renewable penetration

In this case study, we are looking for the optimum HRES with cheapest cost of energy for a site with similar load and renewable resource profiles as in the previous case study. We also add a constraint on the penetration, looking for systems with high renewable penetration ($p \geq 200\%$). Here, by adding a constraint on the penetration of the system we force the optimisation process to reduce the share of the diesel in favour of the share of the renewables.

The obtained optimum configuration for this case study is in agreement with what we expected by forcing the optimisation process toward a high penetration configuration. The

LCE is slightly more than that of CS2 explaining why diesel generator was kept in the configuration through the optimisation process of CS2.

Figure 5 shows the GA search history for this case study. Compared to the GA search histories of CS1 and CS2, a slower convergence rate is observed. This is due to searching within a more constrained design space and using the method of rejection of infeasible solutions.

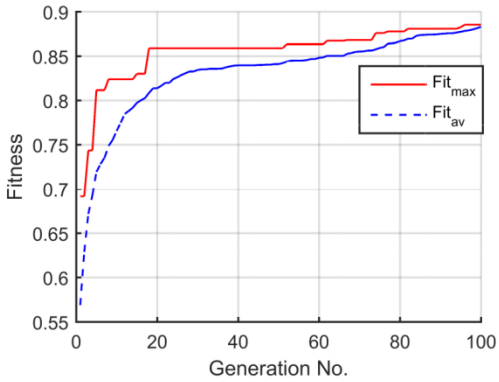

Figure 5-GA search history for CS3

CS4: Size optimisation - fixed configuration

In CS4, the configuration of wind-fuel cell/electrolyser is pre-planned by setting the upper and lower bounds for the size of the other components to zero. This is obviously a non-optimum configuration due to the site's low wind profile and the relatively high LCE of fuel cell/electrolyser compared to other renewable systems. The results show how expensive is this configuration in terms of LCE and TLSC for this site with cost parameters used in this paper, and in fact, explains why there is no fuel cell/electrolyser included in the optimum configurations found in the case studies 1 through 3.

The GA search history is shown in Figure 6. Compared to the search histories of CS1 through CS3, the search history for this case study has no major jumps in the maximum fitness in earlier generations. This was expected as in this case study the configuration is fixed and the major jumps in the earlier generations are due to changes in the configuration (as observed in Figures 2 and 5, and Tables 4 and 5).

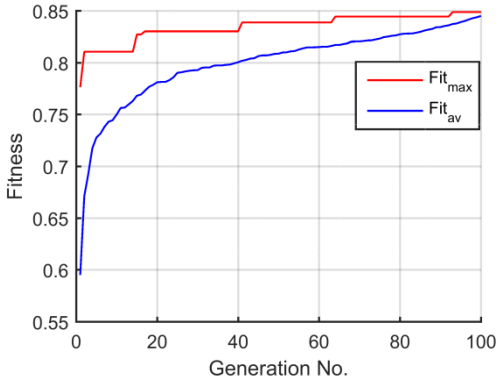

Figure 6-GA search history for CS4

The results of this case study show the flexibility of the problem formulation in dealing with fixed configurations.

CS5: Configuration-size optimisation – retrofitting for saving and environment

In the retrofitting case of CS5 we already have a component with known size and would like to keep it as it is but add new components. In this case the upper and lower limits for diesel generator are set as the nominal size of the existing diesel generator ($P_{D,nom} = 5kW$). Keeping the diesel generator in the configuration as an auxiliary unit reduces the overall cost of the system. However, the usage of the diesel is limited to an annual emission of $CO_2 \leq 500\ kg$. In this case study, since the diesel generator is already in the system, the capital cost (initial cost + installation cost) of the diesel is excluded from the cost analysis.

The search history of Figure 7 shows a slower improvement rate in fit_{max} compared to those of CS1 and CS2. This is due to the presence of the tight constraint on the CO_2 emission.

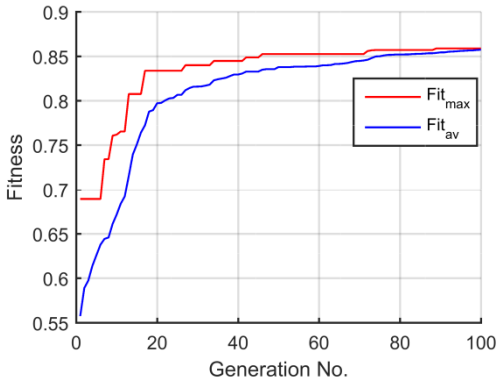

Figure 7-GA search history for CS5

CS6: Size optimisation – retrofitting for investment

In contrary to CS5, in which we retrofitted a given configuration without any constraint on the final configuration, here in CS6, the retrofitting aims at changing a given configuration to a fixed configuration (wind-PV-battery).

The existing 30kW wind turbine installed on Site 1supplies only 71% of the 59.26 MW annual demand while the remaining 17.3 MW is supplied by the grid, which costs $2,760 per year assuming a 16c/kWh flat rate price of electricity from grid. The purpose of retrofitting here is to eliminate the cost of buying electricity from the grid (reduce the unmet load U_t to zero) and to maximise the profit of selling electricity to the grid (assuming a flat rate feed-in tariff of 12c/kWh). The investment budget is limited to $250,000 present value of total lifespan cost.

Similar to CS5, in this case study the capital cost of the wind turbine, as an existing component of the configuration, is excluded from the cost analysis. Unlike the first five case studies, in which infeasible solutions are rejected during the search process, here the constraint of $TLSC \leq 250,000$ makes the design space highly constrained. Therefore, a penalisation strategy is adopted instead. For this problem, different penalty weights were tried to determine the values that put enough pressure on the search to enter the feasible domain before the end of the search. A penalty weight of $\mu_i = 10$ for both constraints was found to be strong enough to lead to feasible solutions. The search history is shown in Figure 8. A low average fitness is observed at earlier generations, which is due to applying high penalties to infeasible solutions.

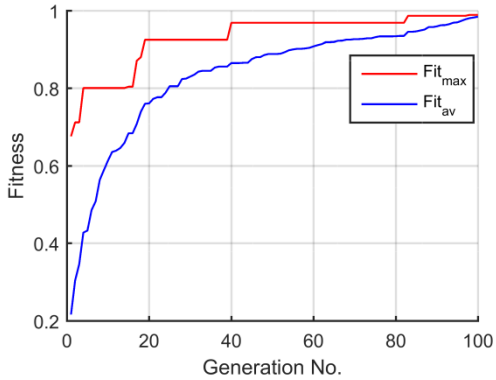

Figure 8-GA search history for CS6

With reference to Figures 2, and 4 through 8, one can observe that in all search histories a good diversity (the distance between fit_{max} and fit_{av} curves) is observed for most of the generations (up to about i_{gen}~80). However, towards the end of the search the diversity starts to decrease rapidly. This is due to the dynamic nature of the designed mutation operator at the size level (Equations 50 to 52). The mutation interval shrinks as i_{gen} increases. Hence, mutation becomes less effective in exploration and more effective in exploitation. An exploitatory mutation together with a crossover, both based on a fitness-based parent selection, lead to a rapid increase in the average fitness. This behaviour is an intended behaviour with the aim of refining the optimum solution towards the end of the search.

The results of case studies 5 and 6 prove the flexibility of the formulation in delivering different cases of retrofitting of existing power systems with adding new constraints or objectives.

CS7: Multiobjective integrated configuration-size optimisation

As mentioned earlier, conducting multiobjective optimisations is the best way to get an insight to the interaction between the design qualities that we are interested in and to select a suitable solution via an informed decision making process. This case study is a multiobjective version of CS1, in which U_t is treated as an objective instead of a hard constraint. Figure 9 and Table 6 show the nondominated solutions for this case study. It should be noted that the constraint $p \geq 60\%$ here is an arbitrary constraint. The purpose of applying arbitrary constraints is to put a focus on part of the design space that we are interested in. For instance, without the constraint $p \geq 60\%$ we would see hundreds of nondominated solutions representing very small systems without any practical use due to very high unmet load.

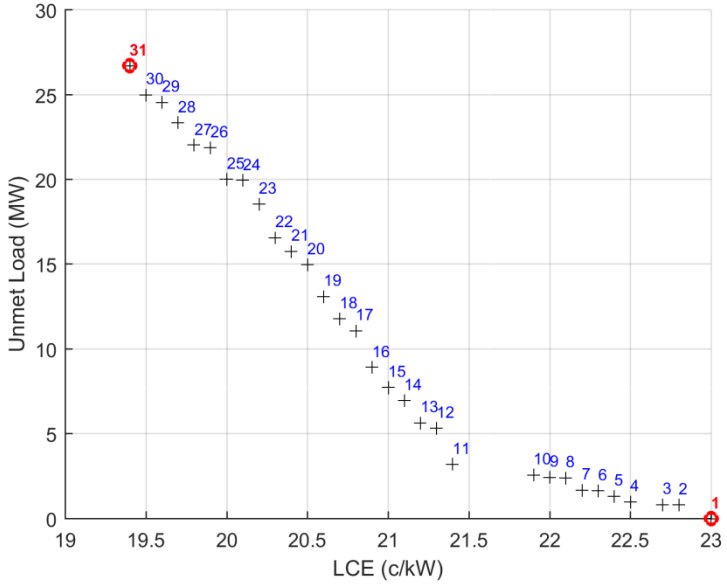

Figure 9-Pareto front of CS7

Table 6-Nondominated solutions of CS7

Sol #	R_{WT} (m^2)	A_{PV} (m^2)	n_B	$P_{D,nom}$ (W)	$P_{FC,nom}$ (W)	$P_{EL,nom}$ (W)	$TLSC$ (1000$)	LCE (c/kWh)	U_t (MW)	p (%)	CO_2 (kg)
1	**0**	**296**	**232**	**0**	**0**	**0**	**186**	**23.0**	**0.00**	**139**	**0**
2	0	289	224	0	0	0	181	22.8	0.83	135	0
3	0	281	232	0	0	0	180	22.7	0.85	132	0
4	0	277	232	0	0	0	178	22.5	1.01	130	0
5	0	271	234	0	0	0	177	22.4	1.34	127	0
6	0	264	238	0	0	0	175	22.3	1.67	124	0
7	0	263	234	0	0	0	174	22.2	1.71	123	0
8	0	254	236	0	0	0	171	22.1	2.43	119	0
9	0	259	224	0	0	0	170	22	2.46	121	0
10	0	256	224	0	0	0	169	21.9	2.60	120	0
11	0	231	214	700	0	0	163	21.4	3.22	108	677
12	0	235	202	0	0	0	156	21.3	5.35	110	0
13	0	232	200	0	0	0	154	21.2	5.66	109	0
14	0	224	196	0	0	0	150	21.1	6.98	105	0
15	0	216	198	0	0	0	147	21	7.74	101	0
16	0	208	194	0	0	0	143	20.9	8.92	97	0
17	0	206	166	0	0	0	136	20.8	11.11	97	0
18	0	194	176	0	0	0	134	20.7	11.81	91	0
19	0	189	166	0	0	0	129	20.6	13.13	89	0
20	0	183	150	0	0	0	123	20.5	14.99	86	0
21	0	183	138	0	0	0	121	20.4	15.78	86	0
22	0	173	144	0	0	0	118	20.3	16.59	81	0
23	0	164	132	0	0	0	112	20.2	18.57	77	0
24	0	157	126	0	0	0	107	20.1	19.95	74	0
25	0	158	122	0	0	0	107	20	20.01	74	0
26	0	148	116	0	0	0	101	19.9	21.88	69	0
27	0	148	112	0	0	0	100	19.8	22.03	69	0
28	0	143	102	0	0	0	96	19.7	23.36	67	0
29	0	136	100	0	0	0	93	19.6	24.56	64	0
30	0	135	94	0	0	0	91	19.5	25.00	63	0
31	**0**	**127**	**86**	**0**	**0**	**0**	**86**	**19.4**	**26.71**	**60**	**0**

Solutions #1 and #31 are the extreme (far-end/boundary) solutions. In a two-dimensional Pareto front, an extreme solution is the best in terms of one objective and the worst in terms of the other objective. Solution #1 $\{U_t, LCE\} = \{0,23\}$ is the best solution in terms of U_t and the worst in terms of LCE. Once the Pareto front is obtained, we can conduct a trade-off study towards selecting a suitable solution. For instance, comparing Solution #12 with the most reliable solution (Solution #1), one can see that \$30,000, one sixth of the $TLSC$, can be saved, if we can tolerate an unmet load of $U_t = 5.35\ MW$, which is only 9% of the total annual demand load of 59.26 MW.

The performance of a multiobjective optimisation method in producing a good approximation of the Pareto front can be assessed by examining two factors: (i) its capability in producing a uniformly populated front and (ii) the (global) optimality of the extreme solutions on that front. With reference to Figure 9, it is evident that the developed NSGA-II meets the first assessment criterion as it produces a fairly uniform and well populated Pareto front. To test the NSGA-II performance in terms of the second assessment criterion, we know that theoretically, the extreme solutions on the actual Pareto front are the results of single objective optimisation problems in which one design quality is considered as objective and the other as constraint. All we need to do is to run two single objective optimisation problems and compare their results with the extreme solutions on the front. The accuracy of the extreme Solution #1 can be examined by solving the single objective problem: $minimise\ LCE$ subject to $U_t = 0$. We already have solved this problem in CS1 and have proved (using exhaustive search) that $\vec{X}_{opt} = \{0,296,232,0,0,0\}$ (see Table 2) is the global optimum, which is identical to the Solution #1 obtained by NSGA-II. This shows that the NSGA-II finds accurate extreme solutions and therefore passes the second assessment criterion.

CS8: Multiobjective configuration-size optimisation - low renewables sites

Nowadays most of renewable technologies have competitive prices compared to fuel-based power systems. As a result of this, in sites with medium to high renewable resources a configuration without diesel generator is probably the optimum solution in terms of the cost of produced energy (for instance, see CS1). For sites with low renewable resources we expect to see diesel in the optimum system configuration. In such cases the environmental impact due to the CO_2 emission needs to be considered alongside the cost and reliability of the system. Site 3 is a low renewable site. Here, we are dealing with three conflicting objectives: a cost related (LCE), a reliability related (U_t), and an environment related (CO_2).

The multiobjective optimisation leads to 81 nondominated solutions. The results of the optimisation are shown in Figure 10. The extreme solutions are identified with coloured circles. In Figure 10 the solution identified with red circle is the best in terms of LCE ($LCE = 29.0\ c/kWh$), those identified with blue circles are the best in terms of U_t ($U_t = 0$), and the green ones are those solutions without diesel generator in the configuration and therefore the best ones in terms of CO_2emission ($CO_2 = 0$).

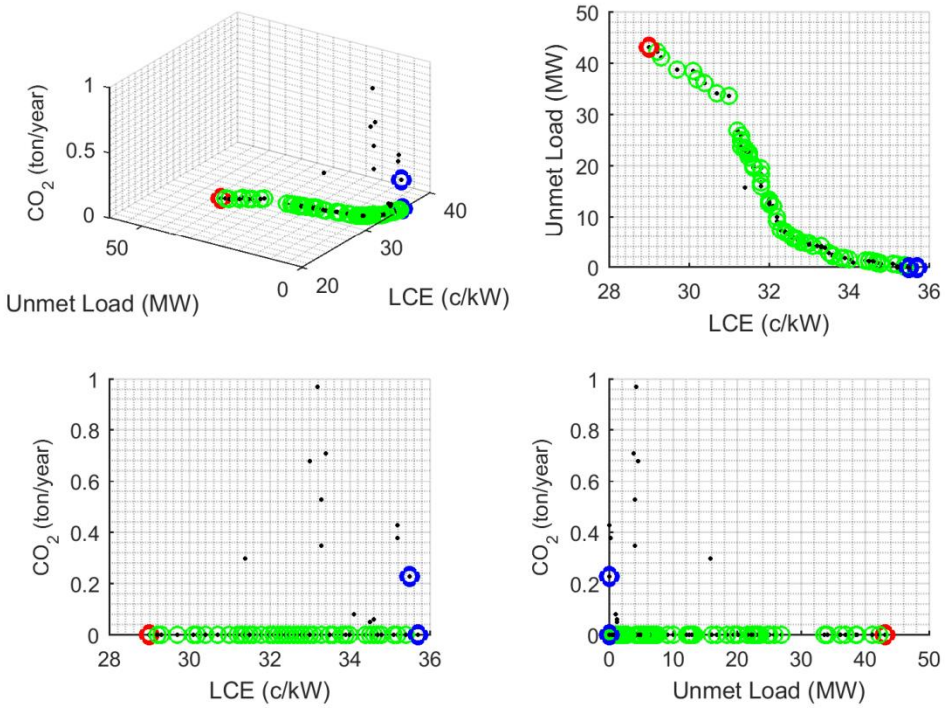

Figure 10-3D Pareto front (top left) and pair-wise fronts of CS8

4.2 Summary of the Results of Case Studies

The results of the case studies prove that the new integrated size-configuration problem formulation has the following features:

- Flexibility: It addition to starting from a generic configuration (which includes all possible components) and leading to the best configuration for a given site (CS1, CS2, CS3, CS7 and CS8), it can also deal with pre-defined (fixed) configurations (CS4), retrofitting of an existing system to a generic configuration (CS5), and retrofitting of an existing system to a fixed configuration (CS6).
- The problem formulation treats all design variables as continuous variables, allowing the manufacturer and provider companies to develop bespoke components for a site to reduce the cost/increase the reliability (e.g. by manufacturing a wind turbine with the required rated power instead of using an existing wind turbine which is overdesigned or under-designed for that site).
- Versatility: It can be easily expanded to include more components than those considered in this paper (wind turbine, PV panel, battery bank, fuel cell, electrolyser and diesel generator), and to include design qualities (objective and constraints) beyond those considered in this paper.

The results also show that the GA reproduction operators which are developed specifically for the problem at hand have the following characteristics:

- Excellent exploitatory functionality at size level: The design space is very vast at the size level. There are 7 design variables, of which 6 of them have a wide range (all but n_{WT}). For instance for the case studies 1, 2, 3, 7 and 8 the lower and upper limits for the design variables are $\vec{X}^l = \{1,0,0,0,0,0,0\}$ and $\vec{X}^u = \{1,22,460,1030,100000,8800,55000\}$ with physical increments of $\{0,0.1,1,\ 1,\ 100,100,\ 100\}$. In order to ensure that the GA

and NSGA-II work efficiently and find optimum/nondominated solutions even with a small population size (in this study 20) and within a small generation number (here 100), the exploitation at the size level must be very efficient. This has been achieved by using a combination of a weighted arithmetic crossover and a dynamic mutation. It was shown that this combination provides excellent exploitation at size level, leading to solutions which match the results of a refined exhaustive search (optimum solution of CS1, and extreme solution of CS7).

- Robust exploratory functionality at size level: The exploratory function is of prime importance for problems with piecewise quality space (see separate surfaces for LCE in Figure 3). A search algorithm with poor exploration capability is more likely to remain on one of the surfaces and therefore to get trapped in a local optima. The search histories of CS1 through CS6, show that the population diversity remains high for most of the generations (indicating a good exploratory functionality), until towards the end of the search where, as intended, the exploitatory functionality of the mutation takes over (fast reduction in the diversity).
- Efficient exploratory functionality at configuration level: Compared to the design space at size level, the design space at configuration level is discrete and limited. Therefore, exploitation is not applicable at configuration level. On the other hand, an efficient exploration at configuration level is very important to have an overall robust optimisation algorithm. An efficient exploration at configuration level allows to identify those configurations which are more likely to be optimum at earlier generations and then, if necessary, to switch between potential optimum configurations as the design space at size level is explored and exploited. Removing components from the configuration (downward change) and adding components to a configuration (upward change) are delivered by a combination of crossover and mutation. The arithmetic crossover can lead to upward change in configuration (but not downward). Mutation can change the configuration both downward and upward. Tables 4 and 5 of case studies CS1 and CS2 show the evolution of the best configuration according to what we expect to see from the planned exploration mechanism at configuration level.
- Capability of handling highly constrained problems: In single objective optimisation formulation, the constraints can be defined on any of the design qualities ($TLSC, LCE, U_t, CO_2, p, feed,$ and $rofit$). This may lead to highly constrained problems, in which penalising infeasible solutions is the only way of evaluating solutions (e.g. as in CS6). Design qualities have different units and different order of magnitudes. The penalty function defined for handling infeasible solutions in highly constrained problems is based on normalised deviations and therefore needs minimal tuning.
- Capability of producing a uniformly populated front and finding the extreme solutions accurately as shown in CS7 and CS8 (for NSGA-II).

5 Concluding Remarks

Sequential configuration-size optimisation, as the current practice, needs a complete size optimisation for all potential configurations that can be made by using all potential components in the system. This can be a cumbersome task when dealing with many potential components. The reported integrated configuration-size optimisation formulation in this paper allows finding the optimum configuration for a given site and the optimum size of each component in that configuration by solving only one optimisation problem. This formulation allows a search within the configuration and size domains simultaneously, hence exploring the overall design space more rigorously, leading to superior solutions.

The integrated configuration-size optimisation formulation presented in this paper can be also used for retrofitting of an existing system, which is another valuable capability of the reported formulation when we design energy transition scenarios. Only an integrated size-configuration formulation allows to incorporate all characteristics of an energy transition scenario, such as adding new sources of energy and new storage systems to the existing system, taking into account an increase in the demand load, and assigning targets to the performance measures (e.g. a targeted reduction in emission).

The integrated configuration-size optimisation formulation requires to be accompanied by a robust search algorithm, which is capable of exploration and exploitation of the design space at configuration and size levels. The developed GA and NSGA-II are proved to be robust in exploration and exploitation of the design space at both configuration and size level. These optimisers can be easily adapted by other researchers and expanded to include more design variables and design qualities.

The generality of the problem formulation and the robustness of the developed optimisers allow for the expansion of the current work beyond power production in future studies, for instance, by integrating heating and thermal storage components and optimal design of combined heat/power systems.

Acknowledgment

The financial support by Energy Renewable UK Ltd through co-funding of REST4U project is gratefully acknowledged.

References

1. Atieh, A., Charfi, S. and Chaabene, M., (2018). Chapter 8 - hybrid PV/batteries bank/diesel generator solar-renewable energy system design, energy management, and economics, In Yahyaoui, I., (Ed.) Advances in Renewable Energies and Power Technologies Elsevier, pp. 257-294.
2. Ismail, M.S., Moghavvemi, M. and Mahlia, T.M.I., (2014). Genetic algorithm based optimization on modeling and design of hybrid renewable energy systems, Energy Conversion and Management, 85, pp.120-130.
3. Samy, M.M., Barakat, S. and Ramadan, H.S., (2018). A flower pollination optimization algorithm for an off-grid PV-fuel cell hybrid renewable system, International Journal of Hydrogen Energy, 44 (4), pp. 2141-2152
4. Senthil Kumar, J., Charles Raja, S., Jeslin Drusila Nesamalar, J. and Venkatesh, P., (2018). Optimizing renewable based generations in AC/DC microgrid system using hybrid nelder-mead – cuckoo search algorithm, Energy, 158, pp.204-215.
5. Mahmoudimehr, J. and Shabani, M., (2018). Optimal design of hybrid photovoltaic-hydroelectric standalone energy system for north and south of Iran, Renewable Energy, 115, pp.238-251.
6. Mohamed, M.A., Eltamaly, A.M. and Alolah, A.I., (2017). Swarm intelligence-based optimization of grid-dependent hybrid renewable energy systems, Renewable and Sustainable Energy Reviews, 77, pp.515-524.
7. Acuna, L.G., Lake, M., Padilla, R.V., Lim, Y.Y., Ponzón, E.G. and Soo Too, Y.C., (2018). Modelling autonomous hybrid photovoltaic-wind energy systems under a new reliability approach, Energy Conversion and Management, 172pp.357-369.

8. Ahmadi, S. and Abdi, S., (2016). Application of the hybrid big Bang–Big crunch algorithm for optimal sizing of a stand-alone hybrid PV/wind/battery system, Solar Energy, 134, pp.366-374.
9. Fetanat, A. and Khorasaninejad, E., (2015). Size optimization for hybrid photovoltaic–wind energy system using ant colony optimization for continuous domains based integer programming, Applied Soft Computing, 31, pp.196-209.
10. Ghorbani, N., Kasaeian, A., Toopshekan, A., Bahrami, L. and Maghami, A., (2018). Optimizing a hybrid wind-PV-battery system using GA-PSO and MOPSO for reducing cost and increasing reliability, Energy, 154, pp.581-591.
11. Jung, J. and Villaran, M., (2017). Optimal planning and design of hybrid renewable energy systems for microgrids, Renewable and Sustainable Energy Reviews, 75, pp.180-191.
12. Kamjoo, A., Maheri, A., Dizqah, A.M. and Putrus, G.A., (2016). Multi-objective design under uncertainties of hybrid renewable energy system using NSGA-II and chance constrained programming, International Journal of Electrical Power & Energy Systems, 74, pp.187-194.
13. Maleki, A., Khajeh, M.G. and Ameri, M., (2016). Optimal sizing of a grid independent hybrid renewable energy system incorporating resource uncertainty, and load uncertainty, International Journal of Electrical Power & Energy Systems, 83, pp.514-524.
14. Muhammad Shahzad Javed, Aotian Song, Tao Ma, (2019). Techno-economic assessment of a stand-alone hybrid solar-wind-battery system for a remote island using genetic algorithm, Energy, Volume 176, 2019, Pages 704-717, https://doi.org/10.1016/j.energy.2019.03.131.
15. Peng, W., Maleki, A., Rosen, M.A. and Azarikhah, P., (2018). Optimization of a hybrid system for solar-wind-based water desalination by reverse osmosis: Comparison of approaches, Desalination, 442, pp.16-31.
16. Tito, S.R., Lie, T.T. and Anderson, T.N., (2016). Optimal sizing of a wind-photovoltaic-battery hybrid renewable energy system considering socio-demographic factors, Solar Energy, 136, pp.525-532.
17. Guangqian, D., Bekhrad, K., Azarikhah, P. and Maleki, A., (2018). A hybrid algorithm based optimization on modeling of grid independent biodiesel-based hybrid solar/wind systems, Renewable Energy, 122, pp.551-560.
18. Chang, K. and Lin, G., (2015). Optimal design of hybrid renewable energy systems using simulation optimization, Simulation Modelling Practice and Theory, 52, pp.40-51.
19. Eltamaly, A.M. and Mohamed, M.A., (2018). 8 - optimal sizing and designing of hybrid renewable energy systems in smart grid applications, pp.231-313.
20. Maheri, A., (2014). A critical evaluation of deterministic methods in size optimisation of reliable and cost effective standalone hybrid renewable energy systems, Reliability Engineering & System Safety, 130pp.159-174.
21. Ogunjuyigbe, A.S.O., Ayodele, T.R. and Akinola, O.A., (2016). Optimal allocation and sizing of PV/wind/split-diesel/battery hybrid energy system for minimizing life cycle cost, carbon emission and dump energy of remote residential building, Applied Energy, 171pp.153-171.
22. Charafeddine Mokhtara, Belkhir Negrou, Noureddine Settou, Belkhir Settou, Mohamed Mahmoud Samy, (2021). Design optimization of off-grid Hybrid Renewable Energy Systems considering the effects of building energy performance and climate change: Case study of Algeria, Energy, Volume 219, 2021, 119605, https://doi.org/10.1016/j.energy.2020.119605.

23. Ramli, M.A.M., Bouchekara, H.R.E.H. and Alghamdi, A.S., (2018). Optimal sizing of PV/wind/diesel hybrid microgrid system using multi-objective self-adaptive differential evolution algorithm, Renewable Energy, 121pp.400-411.
24. Roberts, J.J., Marotta Cassula, A., Silveira, J.L., da Costa Bortoni, E. and Mendiburu, A.Z., (2018). Robust multi-objective optimization of a renewable based hybrid power system, Applied Energy, 223pp.52-68.
25. Wang, R., Li, G., Ming, M., Wu, G. and Wang, L., (2017). An efficient multi-objective model and algorithm for sizing a stand-alone hybrid renewable energy system, Energy, 141pp.2288-2299.
26. Maheri, A., (2016). Effect of dispatch strategy on the performance of hybrid wind-PV-battery-diesel-fuel cell systems, Journal of Thermal Engineering, 2 (4), pp.820-821-825.
27. Sharafi, M. and ELMekkawy, T.Y., (2014). Multi-objective optimal design of hybrid renewable energy systems using PSO-simulation based approach, Renewable Energy, 68pp.67-79.
28. Maleki, A. and Pourfayaz, F., (2015). Sizing of stand-alone photovoltaic/wind/diesel system with battery and fuel cell storage devices by harmony search algorithm, Journal of Energy Storage, 2pp.30-42.
29. Maleki, A., (2018). Design and optimization of autonomous solar-wind-reverse osmosis desalination systems coupling battery and hydrogen energy storage by an improved bee algorithm, Desalination, 435pp.221-234.
30. Gonzalez, A., Riba, J., Esteban, B. and Rius, A., (2018). Environmental and cost optimal design of a biomass–Wind–PV electricity generation system, Renewable Energy, 126pp.420-430.
31. Sawle, Y., Gupta, S.C. and Bohre, A.K., (2018). Socio-techno-economic design of hybrid renewable energy system using optimization techniques, Renewable Energy, 119pp.459-472.
32. Lorestani, A. and Ardehali, M.M., (2018). Optimization of autonomous combined heat and power system including PVT, WT, storages, and electric heat utilizing novel evolutionary particle swarm optimization algorithm, Renewable Energy, 119pp.490-503.
33. Maheri, A., (2014). Multi-objective design optimisation of standalone hybrid wind-PV-diesel systems under uncertainties, Renewable Energy, 66pp.650-661.
34. Baghaee, H.R., Mirsalim, M., Gharehpetian, G.B. and Talebi, H.A., (2016). Reliability/cost-based multi-objective pareto optimal design of stand-alone wind/PV/FC generation microgrid system, Energy, 115pp.1022-1041.
35. Ekoh, S., Unsal, I. and Maheri, A., (2016). Optimal sizing of wind-PV-pumped hydro energy storage systems, 2016 4th International Symposium on Environmental Friendly Energies and Applications (EFEA), Belgrade, Serbia, pp. 1-2-6.
36. Sharafi, M., ElMekkawy, T.Y. and Bibeau, E.L., (2015). Optimal design of hybrid renewable energy systems in buildings with low to high renewable energy ratio, Renewable Energy, 83pp.1026-1042.
37. Gan, L.K., Shek, J.K.H. and Mueller, M.A., (2016). Optimised operation of an off-grid hybrid wind-diesel-battery system using genetic algorithm, Energy Conversion and Management, 126pp.446-462.
38. Maleki, A. and Rosen, M.A., (2017). Design of a cost-effective on-grid hybrid wind–hydrogen based CHP system using a modified heuristic approach, International Journal of Hydrogen Energy, 42(25), pp.15973-15989.
39. Morshed, M.J., Hmida, J.B. and Fekih, A., (2018). A probabilistic multi-objective approach for power flow optimization in hybrid wind-PV-PEV systems, Applied Energy, 211pp.1136-1149.

40. Kahwash, F., Maheri, A., Mahkamov, K. (2021). Integration and Optimisation of High-Penetration Hybrid Renewable Energy Systems for Fulfilling Electrical and Thermal Demand for Off-grid Communities. Energy Conversion and Management, vol. 236, 114035 https://doi.org/10.1016/j.enconman.2021.114035
41. Assaf, J. & Shabani, B. (2019). A novel hybrid renewable solar energy solution for continuous heat and power supply to standalone-alone applications with ultimate reliability and cost effectiveness. Renewable Energy, vol. 138, pages 509-520. https://doi.org/10.1016/j.renene.2019.01.099
42. Henrik Lund (2018). Renewable heating strategies and their consequences for storage and grid infrastructures comparing a smart grid to a smart energy systems approach. Energy, vol 151, pages 94-102. https://doi.org/10.1016/j.energy.2018.03.010
43. Henrik Lund, Poul Alberg Østergaard, David Connolly, Brian Vad Mathiesen (2017). Smart energy and smart energy systems. Energy, vol 137, pages 556-565. https://doi.org/10.1016/j.energy.2017.05.123
44. Henrik Lund, Poul Alberg Østergaard, David Connolly, et al (2016). Energy Storage and Smart Energy Systems. International Journal of Sustainable Energy Planning and Management vol. 11, pages 3-14.
45. Henrik Lund, Jakob Zinck Thellufsen, Poul Alberg Østergaard, et al (2021). EnergyPLAN-Advanced analysis of smart energy systems. Smart Energy, vol 1, 100007, https://doi.org/10.1016/j.segy.2021.100007
46. Rodolfo Dufo-López, José L. Bernal-Agustín, Multi-objective design of PV–wind–diesel–hydrogen–battery systems, Renewable Energy, Volume 33, Issue 12, December 2008, pp. 2559-2572.
47. Yi He, Su Guo, Jianxu Zhou, Feng Wu, Jing Huang, Huanjin Pei, (2021). The many-objective optimal design of renewable energy cogeneration system, Energy, Volume 234, 2021, 121244, https://doi.org/10.1016/j.energy.2021.121244.
48. Marek Jaszczur, Qusay Hassan, Patryk Palej, Jasim Abdulateef, (2020). Multi-Objective optimisation of a micro-grid hybrid power system for household application, Energy, Volume 202, 2020, 117738, https://doi.org/10.1016/j.energy.2020.117738.
49. Althani, M. H. A., Maheri, A. (2021). An Ant Colony Algorithm for HRES Size and Configuration Optimisation. In the proceedings of the 6th International Symposium on Environment Friendly Energies and Applications. IEEE Explore. https://doi.org/10.1109/EFEA49713.2021.9406256
50. F. Kawash, A. Maheri "Updated cost modeling of hybrid renewable energy system components". in 1st International Conference on Engineering of Tarumanagara, ICET 2013.
51. O. Schmidt, A. Gambhir, I. Staffell, A. Hawkesc, J. Nelson, S. Few (2017). Future cost and performance of water electrolysis: An expert elicitation study, International Journal of Hydrogen Energy, 42 (52), pp.: 30470-30492
52. MOHRES www.mohres.com
53. Maheri, A. (2021) MOHRES, a Software Tool for Analysis and Multiobjective Optimisation of Hybrid Renewable Energy Systems: An Overview of Capabilities. In the proceedings of the 6th International Symposium on Environment Friendly Energies and Applications. IEEE Explore. https://doi.org/10.1109/EFEA49713.2021.9406221

Appendix

Table A.1-The remaining power and cost modelling parameters

Parameter (unit)	Value
Margin of safety (storage sizing) $MOS(-)$	0.2

Autonomy period (battery sizing) $T_{a,B}$ (day)	1
Autonomy period (H2 tank sizing) T_{a,H_2} (day)	0.5
Air density ρ (kg/m^3)	1.225
Overall wind turbine mechanical and electrical efficiency η_{EM} (%)	90
Site surface roughness length z_0 (m)	0.03
Minimum blade tip-ground clearance h_c (m)	8
Wind turbine hub elevation for pre-sizing calculations $h_{hub,0}(m)$	12
PV panel efficiency η_{PV} (%)	14
Battery nominal capacity per unit battery c_B (Ah)	40
Battery bank voltage $V_B(V)$	24
Battery maximum SOC, SOC_{max} $(-)$	1
Battery minimum allowable SOC, SOC_{min} $(-)$	0.5
Battery efficiency in charge $\eta_{B,c}$ (%)	90
Battery efficiency in discharge $\eta_{B,d}$ (%)	95
Battery self-discharge rate, δ (%)	0.2
Fuel cell efficiency η_{FC} (%)	47
Electrolyser efficiency η_{EL} (%)	74
Diesel generator fuel cost C_{fuel} $(\$/l)$	1
Emission per litre of diesel $CO_2(kg)$	2.68
System nominal life N_S $(years)$	20
Real discount rate d (%)	4

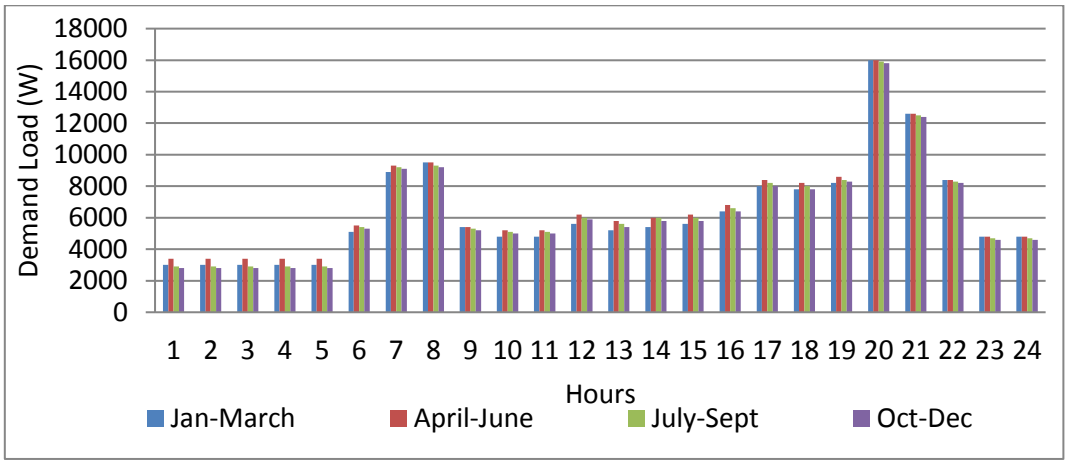

Figure A1-Hourly averaged demand load for four seasonal typical days

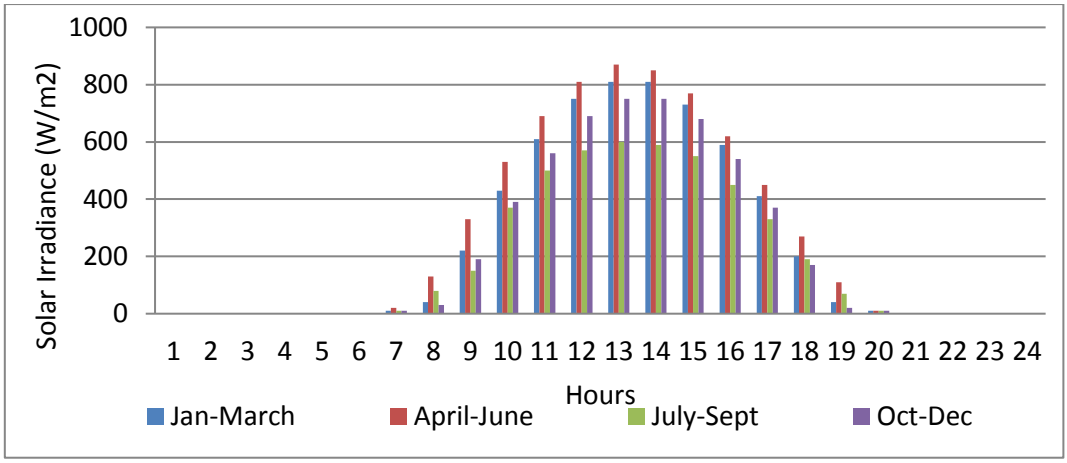

Figure A2-Hourly averaged solar irradiance for four seasonal typical days

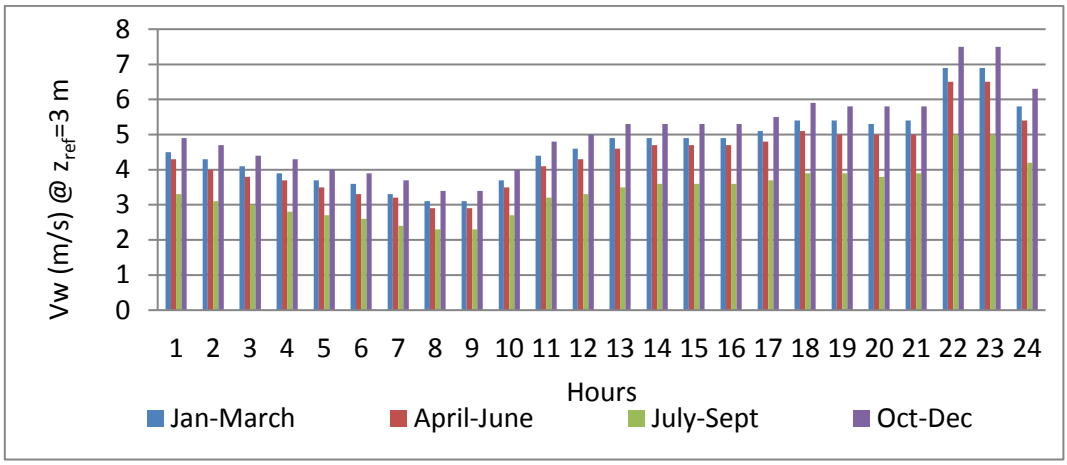

Figure A3-Hourly averaged wind speed for four seasonal typical days at a reference height of $z_{ref} = 3m$